Turkish Journal of Physics

Volume 35 | Number 2 Article 2

1-1-2011

A Quantum theory of the scattering of soft x-ray from Compton effect caused electron standing wave in the materials

BISWAJIT MALLICK

Turk J Phys
35 (2011) , 75 – 114.

doi:10.3906/fiz-1101-81

A Quantum theory of the scattering of soft x-ray from Compton effect caused electron standing wave in the materials

Biswajit MALLICK
Institute of Physics, Bhubaneswar 751005, INDIA
e-mail: bmallick_iopb@scientist.com

Received: 02.01.2011

Abstract

In the present investigation, low-energy x-rays ($<$ 15 keV) scattered from powder, polymer, crystals and hydrogenous liquids (with preference for materials of low binding energy) at different scattering angles have been analysed. The scattered x-rays show unambiguous existence of a new modified line along with unmodified and Compton line. Since, the experimental observation of the inverse Doppler effect, i.e. increase of frequencies of reflecting waves from a receding boundary, has already been reported [Seddon and Bearpark (2003) *Science*, **302**, 1537–1540]. Hence, it is quite logical to think that x-rays may also gain energy in contrast to Compton effect (where they lose energy) in material medium. Such type of new modified x-ray scattering (angle dependent) was observed. Expressions for photon of enhanced energy, $\hbar\omega_3$, initial momentum of plasmon q' and the total scattering cross section σ_N of this new phenomenon have been derived. The σ_N is found out to be proportional to $\sqrt{\in}$ and is about 100 times less than the Compton cross section using high-energy x-ray photon (100's of keV), usually used for Compton scattering studies. Both theoretically calculated and experimentally observed data match well with one another. The new modified line is to be clearly expected from materials of low atomic number with high dielectric constant using low-energy x-rays.

Key Words: X-ray scattering, Compton effect, plasmon excitation, inverse Doppler effect

PACS: 78.70.Ck, 78.70.-g, 71.45.Gm, 81.05.Xj, 71.20.Rv

1. Introduction

Discovered in 1921, Compton scattering [1] is used to measure the electron momentum distribution of atoms [2–8]. Subsequently, Smekal-Raman [9, 10] and plasmon scattering [11] were discovered. Moreover, Stokes and anti-Stokes lines were observed using both light and x-rays [12]. A number of good works on incoherent scattering of radiation by plasma have already been reported by various authors [13–20]. Existence of inverse Compton [21, 22], virtual Compton [23], magnetic Compton [24], double Compton [25], and resonant Compton

[26] scattering were reported. Experimental verification of inverse Doppler effect [27] has been reported recently in 2003. Electrons [28–32], protons [33–35], and neutrons [36–40] used as a probe instead of photons in Compton scattering have also been reported. As nature loves symmetry, it is quite logical to think that x-rays may also exhibit inverse Doppler effect, where they gain energy in contrast to Compton effect (where they lose energy) in material medium. Non-observance of this type of incoherent scattering peak in the earlier Compton scattering experiments may be due to the following reasons: (i) most of the earlier Compton scattering work was restricted to relatively hard radiation and large scattering angle; (ii) the plasmon excitation in Compton scattering was discovered nearly 50 years after the discovery of Compton scattering; (iii) the damping of the plasmon increases with momentum transfer k $(= \ (4\pi/\lambda) \ \sin\theta)$ [11], which is directly proportional to radiation energy and scattering angle; (iv) intensity ratio of the new incoherent peak with unmodified peak was a few tens of times less than the intensity ratio of Compton peak with unmodified peak; (v) sample gets heated due to long exposure to x-ray and the Compton peak decreases slightly when this temperature increases, hence the new peak intensity decreases [41]; (vi) the new scattering was masked by Compton tail of the neighbouring incident x-ray line, spurious peaks, and peak due to source fluctuation; (vii) most of the earlier workers were interested in low-energy side (Compton region) of the unmodified peak; and (viii) the number of photons emitted per second was much less in x-ray sources used in earlier experiments [42]. Thus, the observation of inverse Doppler effect in x-ray was completely sidetracked.

A few years ago, the author observed the scattered x-rays of enhanced energy from solid polymer and suggested that it is because of collision of incident photons with Compton recoil electrons (classical treatment) [43–45]. However, it was not clear in those days; the reason may be lack of negative refractive index concepts in the scattering. However, recent, experiments have shown the existence of such type of incoherent scattering which matches well with the predicted quantum mechanical model.

Schrödinger in 1927 formulated a wave-mechanical model using simple de Broglie's concepts of matter waves for the Compton scattering [46], which leads precisely to the same result for the change in wavelength of scattered x-rays as that derived on the theory of impact between photon and free electron by Compton. This quantum mechanical theory doubtlessly gives a more adequate picture of the wavelength change as follows. Consider a new coordinate system where impact of photon and electron are symmetrical both before and after the collision. If v is the velocity of the electron's recoil ($v << c$) in the fixed co-ordinate, then the required velocity of the moving coordinate is $v/2$. At the impact, the momentum of the electron then changes from $-mv/2$ to $+mv/2$ as expressed in the moving system, while Y-component of the photon's momentum changes from $+(h/\lambda) \ \sin\theta$ to $-(h/\lambda) \ \sin\theta$. Thus, the condition for the momentum conservation [46] gives

$$-(m_0 v/2) + (h/\lambda) \ \sin\theta \ = \ (m_0 v/2) \ - (h/\lambda) \ \sin\theta \tag{1}$$

$$(2h/\lambda) \ \sin\theta \ = \ m_0 v. \tag{2}$$

Thus the energy remains unchanged after impact. Applying Schrödinger and de Broglie hypothesis, the incident electron can be represented by a continuous train of ψ waves of wavelength $\lambda_{matter} = \ h/(m_0 v/2)$ moving along negative y-direction and the recoil electron (atomic) by a similar train of the same wavelength moving along positive y-direction, the two trains together will form standing waves for which the electronic charge density is proportional to $\psi_{inc}\psi^*_{rec}$ and for which the distance from the node to node is $(\lambda_{matter}/2) = \ h/(m_0 v)$. The de Broglie waves representing the electron thus form a Bragg grating space $d = h/(m_0 v)$. This grating will diffract the incident x-ray waves according to the usual expression $-2d \sin\theta = \lambda$. The diffracted waves are modified in

wavelength by the deflection because the grating is in motion, thus resulting in a Doppler effect. Considering the fixed coordinate system as in Figure 1(a), the grating of stationary de Broglie waves is receding from O with velocity $v/2$. Treating grating as a mirror, this is equivalent to receiving the light from a virtual image of the source S that recedes from S with velocity v. According to the Doppler's principle, the modified wavelength emitted from S and reaching P can be written as $\lambda' = \lambda\,(1 + (v/c)\,\sin\theta)$. Substituting the value of v from equation (2), the increase in wavelength can be simplified as

$$\Delta\lambda_C = (2h/mc)\sin^2\theta \;=\; (h/m_0c)\;(1-\cos 2\theta) \tag{3}$$

which is exactly the same expression as that obtained from photon theory given by Compton and is known as Compton shift, where 2θ is the scattering angle.

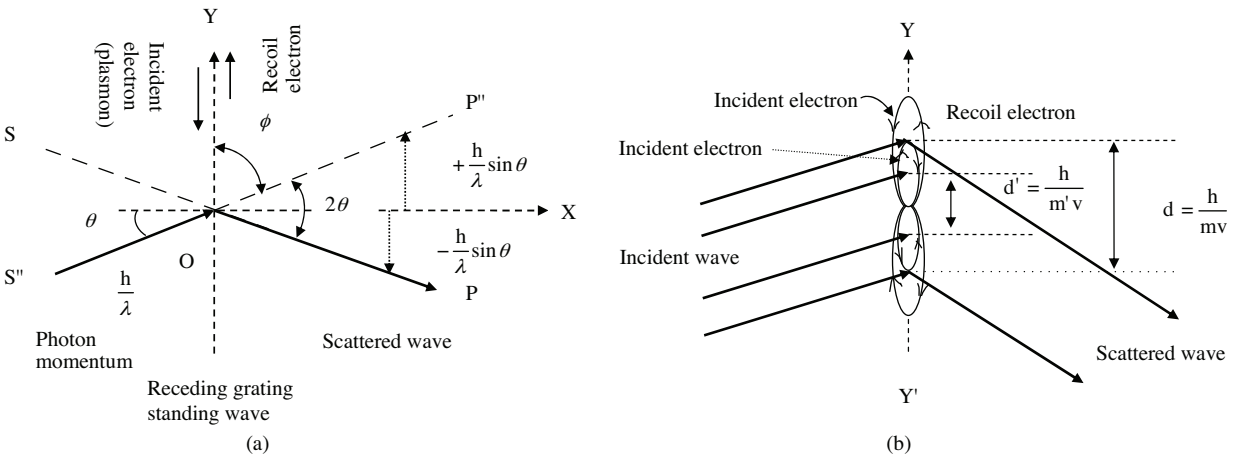

Figure 1. Schematic diagram of. (a) collision of a photon and electron (or plasmon) in normalized coordinates, (b) diffraction of incident waves from the standing wave pattern due to incident electron ($d = h/(mv)$) or plasmon ($d' = h/(m'v')$) and recoil electrons. The incident wave diffracted from the normal dispersion media (v_{group} and v_{phase} are parallel, positive refractive index) due to incident electron standing wave shows scattered wave of lower frequency. Again, incident wave diffracted from the anomalous dispersive media (v_{group} and v_{phase}, are anti-parallel, negative refractive index) due to incident plasmon standing wave possesses scattered wave of higher frequency.

2. Hypothesis

Substances with negative permittivity ε and permeability μ have some properties which differ from those of substances with positive ε and μ. In solid-state plasmas ($\varepsilon < 0$, $\mu > 0$), the square of the refractive index (RI), i.e. n^2 becomes negative, which leads to reflection of waves from such a medium [47]. Again, due to plasmon excitation in the solid because of Compton effect, material behaves as a metamaterial. The plasmon frequency can be defined as $\omega_p^2 = e^2 n_e/\ (\varepsilon_0\ \ m^*)$, where n_e is the electron density (electrons/cm^3), e is the electronic charge, ε_0 is the permittivity of free space (dielectric constant) and m^* is the effective mass of electron. The total number of electrons N_e in the target can be defined as $N_e = \pi\ (\frac{d}{2}\ )^2\ l\ \rho\ \frac{N_A}{A}\ Z$, where d is the diameter of target, l is the length of the target (length of the target intercepted by the beam), ρ is

the density of the target material, N_A is the Avogadro's number (6.023×10^{23}), A is the atomic weight of the target element and Z is the atomic number of the element [48].

Again, the critical electron density [49] is defined as $n_c = \varepsilon_0 m^* \omega^2/e^2$. However, dielectric function [50] or permittivity of the medium is usually expressed as $\varepsilon(\omega) = 1-(\omega_p^2/\omega^2)$, whence using the value of ω^2, critical plasmon density can be simplified in terms electron density as

$$n_c = (\varepsilon_0 m^* \omega_p^2)/e^2\ (1-\varepsilon_) = n_e/(1-\varepsilon). \tag{4}$$

Simplifying equation (4) for ε, and taking the square root of both sides of the expression, gives $\sqrt{1-(n_e/n_c)} = \sqrt{\varepsilon}$. Again, $\varepsilon = \varepsilon_0 \in$, where ε_0 $(=1/4\pi)$ is the permittivity of free space and $\in$ is the dielectric constant of the material. So above-mentioned relationship can be simplified as

$$\sqrt{1-(n_e/n_c)} = \sqrt{\varepsilon_0 \in} = \pm R, \tag{5}$$

where R is a constant. The RI of the plasmon [49] can be defined as$n = \sqrt{1-(n_e/n_c)}$, since for x-rays $n_c >> n_e$,$n = 1-(n_e/2\,n_c)$, hence from equation (5) the RI can be written as

$$n = 1-(n_e/2\,n_c) = \pm R. \tag{6}$$

It is clear from the above that, if $n_c <<$, RI becomes negative. Also, n is directly proportional to R $(=\sqrt{\varepsilon_0 \in})$ or $\sqrt{\in}$. The numerical factor R increases with a higher value of $\in$. Again, for x-ray of wavelength λ, the plasmon critical density [51] can be defined as $n_c = \pi/(r_0\lambda^2)$, where r_0 is the classical electron radius and the relation show that if the wavelength of x-ray increases (low energy), n_c will decrease, hence RI of the material moves towards negative. So, for the negative refractive index (NRI), i.e. n = - R, material behaves as a metamaterial. x-ray reflected from the standing wave pattern receding in the solid-state plasma media (virtual metamaterial), generated because of Compton effect, produces waves of increased frequency. For a wave (x-ray) traveling in normal dispersive media (stationary frame of reference) incident on a receding grating, the receding grating velocity or group velocity (v_{group}) and the phase velocity (v_{phase}) of the incident wave (x-ray) are parallel therefore, the incident field in the frame of the receding grating oscillates with a relatively low frequency as expected for conventional Doppler effect shown in Figure 1(b). In the anomalously dispersive medium (solid-state plasmon), the v_{phase} of the incident wave and v_{group} are anti-parallel. In this case the incident field in the frame of receding grating (in excited electron/plasma medium) oscillates with a relatively high frequency as expected for the inverse Doppler effect. Again RI is given as $n = c/v_{phase}$, which shows that for NRI material (solid-state plasma) the phase velocity becomes negative and $v_{group} = c^2/(\pm v_{phase})$, so the receding velocity. If v' is the velocity of standing wave ($v' << c$) formed due to recoil (ejected) electron (Compton effect) and plasmon in the fixed coordinate system, then the receding velocity in the moving coordinate system is$v'/2$. The de Broglie waves representing the plasmon thus form a Bragg grating space $d' = h/(m'v')$, where $d' < d$. Similarly, the momentum of the electron then changes from $--m'v'/2$ to $+m'v'/2$ as expressed in the moving system. As per equations (1) and (2), one can have

$$(2h/\lambda)\ \sin\theta = m'v'. \tag{7}$$

According to general theory of relativity and de Brogile hypothesis, energy of exited electrons can be expressed

as $E = E_0/\sqrt{1-(v'/c)^2}$, so

$$\frac{v'}{c} = \sqrt{1-(E_0/E)^2}, \tag{8}$$

where E_0 $(= m_0c^2)$ is the rest-mass energy of the electron, and $E = m'c^2 = E_0 + \Delta E$, ΔE is the amount of energy gained by the electron in collision process. The mass in terms of energy can be written as

$$m' = m_0(E/E_0). \tag{9}$$

Similarly, according to the Doppler's principle, the new modified wavelength of the radiation can be defined as $\lambda'' = \lambda\,(1-(v'/c)\,\sin\theta)$. Further simplifying the above relation for solid-state plasmon system by substituting the value of v' from equation (7) and m' from equation (9), the change (decrease) in wavelength can be written as

$$\Delta\lambda_N \;= [2h/\,(m_0(E/E_0)\;c)]\;\sin^2\theta \;=\; (h/m_0\;c)\;(E_0/E)\;\;(1-\cos 2\theta) \tag{10}$$

The energy enhancement in this new effect is of the same order as the amount of energy absorbed in Compton process.

3. Theory

In a typical x-ray Compton scattering experiment, a beam of monochromatic radiation with energy ω_1 and momentum k_1 is incident on a target consisting of a set of scatterers. The radiation is scattered through an angle 2θ with respect to the incident beam direction. The scattered radiation of energy ω_2 and momentum $k_2(\hbar = 1)$ is analysed. The various steps of interaction mechanism are discussed below.

3.1. Electron at rest

If the electron of the scatterer is supposed to be at rest and free, then from the energy momentum conservation laws we have

$$\hbar\omega_1 = \hbar\omega_2 + \left(\hbar^2k^2/2m_0\right), \tag{11}$$

where

$$k = k_1 - k_2. \tag{12}$$

Here k is the scattering vector, and k_i $(i = 1, 2)$ are the wave vectors having magnitude $|k_i| = 2\pi/\lambda_i$. The energy transferred to the system in this process is

$$\Delta\hbar\omega = \hbar\omega_1 - \hbar\omega_2 = \left(\hbar^2k^2/2m_0\right). \tag{13}$$

In terms of the scattering angle 2θ,

$$k^2 = (k_1 - k_2)^2 \;= k_1^2 + k_2^2 - 2k_1k_2\;\cos\,2\theta. \tag{14}$$

Typically, the energy of the x-ray photon is usually very high compared to its momentum. So, to a first approximation $|k_1|^2 \approx |k_2|^2$, so

$$k^2 = 2k_1^2 - 2k_1^2\;\cos 2\theta = 2k_1^2\,(1-\cos 2\theta). \tag{15}$$

Since, $\omega_1 = k_1 c$ and $\omega_2 = k_2 c$, equation (13) may be written as

$$\Delta\hbar\omega = \left(\hbar^2\omega_1\omega_2/m_0c^2\right)\ (1-\cos 2\theta) \tag{16}$$

This gives the final energy of the Compton scattered x-ray photon as

$$\hbar\omega_2 = \frac{\hbar\,\omega_1}{[1+\gamma\ (1-\cos\ 2\theta)]}, \tag{17}$$

where $\gamma = \frac{\hbar\,\omega_1}{m_0c2}$ is the ratio of the incident photon energy with respect to rest mass energy of electron.

In other words, the change in wavelength of the x-ray photon is the same as defined in earlier expression (3).

3.2. Electron in motion

For an electron in motion, equation (11) is slightly modified to

$$\hbar\omega_1 + \left(p_1^2/2m_0\right) = \hbar\omega_2 + \left(p_2^2/2m_0\right) \tag{18}$$

and

$$\hbar k_1 + p_1 = \hbar k_2 + p_2; \tag{19}$$

or,

$$p_2 = p_1 + \hbar k, \tag{20}$$

where p_1 and p_2 are the initial and final momentum of the electron, respectively.

Using equations (18) and (20), the amount of energy transferred to electrons may be written as

$$\begin{aligned}\Delta\hbar\omega = \hbar\omega_1 - \hbar\omega_2 &= \left(p_2^2/2m_0\right) - \left(p_1^2/2m_0\right)\\ &= \left(\left(p_1+\hbar k\right)^2/2m_0\right) - \left(p_1^2/2m_0\right);\end{aligned}$$

so,

$$\Delta\hbar\omega = \left(\hbar^2k^2/2m_0\right) + \left(\hbar k\cdot p_1/m_0\right). \tag{21}$$

Here, $\mathbf{k}$ is the scattering vector (Figure 2(a)); and for a fixed k, the energy resolution is linearly related to the momentum resolution. It is conventionally chosen as the z-axis of a Cartesian coordinate system. In addition to equation (16), equation (21) now contains an extra term which is linearly dependent on one component p_z of the electrons ground state momentum and the Doppler shift associated with electron in motion. The Compton profile (CP) is centered around $k^2/2m_0$ with a width $k\cdot p_1/m_0$.

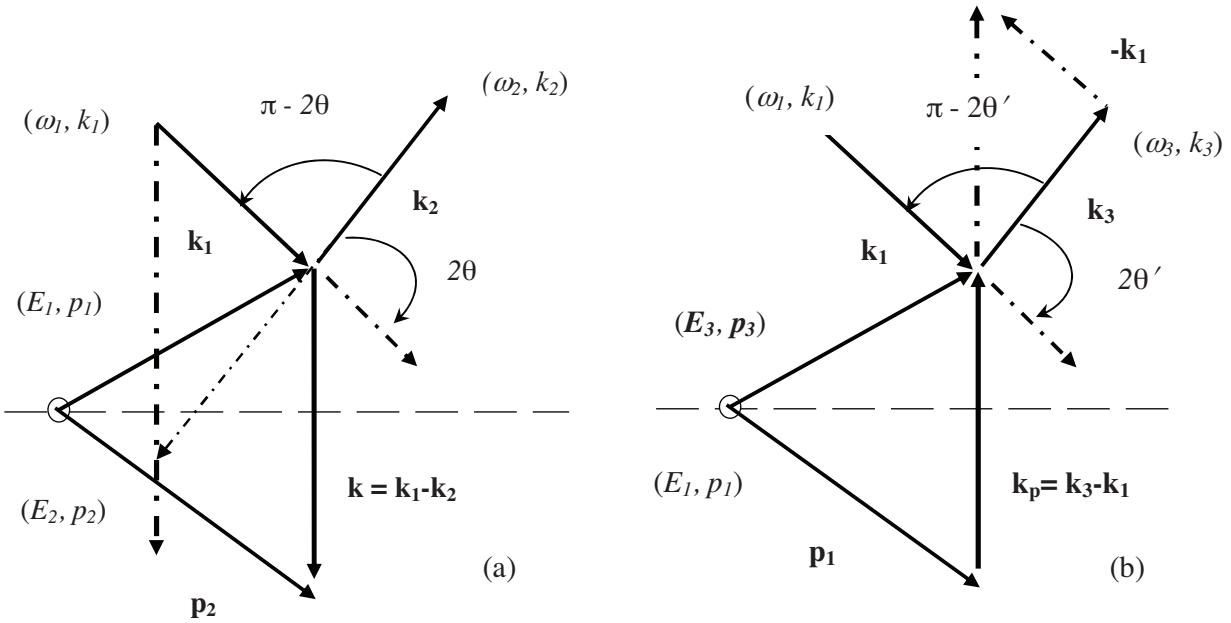

Figure 2. Schematic diagram of. (a) Compton process showing momentum conservation, where $\mathbf{p}_1$ and $\mathbf{p}_2$ are the initial and final momenta of the electron, $\mathbf{k}_1$ and $\mathbf{k}_2$ of the x-ray photon. E_1, and E_2, are the initial and final energy of the electron, ω_1 and ω_2 of the x-ray photon. The $\mathbf{k}$ is the scattering vector recedes from the collision centre; (b) new scattering process showing momentum conservation where $\mathbf{p}_3$ and $\mathbf{p}_1$ are the initial and final momenta of the excited electron (plasmon) due to Compton effect, $\mathbf{k}_1$ and $\mathbf{k}_3$ of the x-ray photon. E_3, and E_1, are the initial and final energy of the plasmon, ω_1 and ω_3 of the x-ray photon. The $\vec{k}_p$ is the scattering vector approaching to the collision centre.

Hence, we have:

$$\Delta\hbar\omega = (\hbar\omega_1 - \hbar\omega_2) + (\hbar k p_1/m_0)$$

or,

$$\hbar\omega_2 = \hbar\omega_1 - \Delta\hbar\omega + (\hbar k p_1/m_0)$$

or,

$$\hbar\omega_2 = \hbar\omega_1 - \left(\hbar^2\omega_1\omega_2/m_0c^2\right)\,(1-\cos 2\theta) + (\hbar k p_1/m_0)$$

or,

$$\hbar\omega_2\left(1 + \left(\hbar\omega_1/m_0c^2\right)\,(1-\cos 2\theta)\right) = \hbar\omega_1 + (\hbar k p_1/m_0)\,. \tag{22}$$

Again, the term $\frac{\hbar}{m_0}\,kp_1$ in equation (22) can be simplified using equation (15) as

$$\frac{\hbar}{m_0}\,kp_1 = \frac{\hbar}{m_0}\,\sqrt{2k_1^2(1-\cos 2\theta)}\cdot m_0 v,$$

$$\frac{\hbar}{m_0}\,kp_1 = \frac{\hbar}{m_0}\,\left(2\,\left(\frac{\omega_1}{c}\right)\,\sqrt{\sin^2\theta}\right)\cdot m_0 v = 2\,\hbar\omega_1\left(\frac{v}{c}\right)\,\sqrt{\sin^2\theta}. \tag{23}$$

Finally, from equation (22) and (23)

$$\hbar\omega_2 = \frac{\hbar\,\omega_1}{[1+\gamma\,\,(1-\cos\,\,2\theta)]} + \frac{2\,\hbar\omega_1\left(\frac{v}{c}\right)\,\sqrt{\sin^2\theta}}{[1+\gamma\,\,(1-\cos\,\,2\theta)]}. \tag{24}$$

The second term of the above equation (24) is the width of the Compton band in terms of energy. Here, expressing equation (24) in terms of wavelength shift, we have

$$\delta\lambda_{\,c} = (2h/m_0c)\sin^2\theta \;+\; 2\,(\lambda\,\lambda')^{\frac{1}{2}}\,(p_z/m_0c)\,\sin\theta. \tag{25}$$

3.3. Electron in oscillating state

In Compton effect, a photon of energy $\hbar\omega_1$, scattered through an angle 2θ from materials consisting of set of rest and free electrons having initial momentum p_1, becomes a scattered photon of reduced energy $\hbar\omega_2$. These rest and free electrons absorb the amount of energy lost by the photon scattered with a momentum p_2. Hence, there is a vacancy in the atomic orbit. However, the number of positive charges in the centre remains constant. Then the electron density fluctuation takes place. Hence the excited oscillatory motion of fluctuating bound electrons possesses a new momentum p_3. These excited electrons, after transforming energy to another incident x-ray photon, attain a relaxed state of momentum p_1', which is nearly the same as the initial momentum p_1. X-ray photon scattered from the above oscillating electrons (solid-state plasmon) shows a new type of incoherent scattering of enhanced energy $\hbar\omega_3$. From energy momentum conservation laws we have

$$\hbar\omega_1 + \left(p_3^2/2m_0\right) = \hbar\omega_3 + \left(p_1'^2/2m_0\right) \tag{26}$$

and

$$\hbar k_1 + p_3 = \hbar k_3 + p_1' \tag{27}$$

or,

$$p_3 = \hbar k_3 - \hbar k_1 + p_1, [p_1' = p_1], \tag{28}$$

where p_3 and p_1 are the initial and final momentum of excited plasmon, respectively, k_3 is the final momentum of new scattered photon, and $k_p = k_3 - k_1$ is the scattering vector shown in Figure 2(b). The amount of energy transferred to x-ray photon from excited electron (plasmon) may be written as

$$\begin{aligned}\Delta\hbar\omega|_N &= \hbar\omega_3 - \hbar\omega_1 = \left(p_3^2/2m_0\right) - \left(p_1^2/2m_0\right)\\ &= \left(p_1 + \hbar k_p\right)^2/2m_0 - \left(p_1^2/2m_0\right),\end{aligned}$$

so,

$$\Delta\hbar\omega|_N = \left(\hbar k_p + p_1\right)^2/2m_0 - \left(p_1^2/2m_0\right),$$

or,

$$\Delta\hbar\omega|_N = \left(\hbar^2 k_p^2/2m_0\right) + \left(\hbar k_p.p_1/m_0\right), \tag{29}$$

which is similar to equation (21). Now, the equation (29) contains an extra term, which is also linearly dependent on the electrons ground state momentum and the inverse Doppler shift associated with electron in plasmon excitation. Hence, the new profile of the scattered photon is centred on $k_p^2/2m_0$ with a width $k_p \cdot p_1/m_0$.

As it is difficult to detect the scattered electron experimentally, one can only record the energy distribution of the Compton scattered x-ray photons and then infer the momentum distribution of the electron. In order to extract the information regarding the momentum of the scattering electron, let us define

$$q = k \cdot p \;/\; |k|, \tag{30}$$

which is the projection of the momentum p onto the scattering vector k. From equation (22), one can get after slight modification

$$(\hbar k.p_1/m_0) = -\hbar\omega_1 + \hbar\omega_2 \left(1 + \left(\hbar\omega_1/m_0c^2\right)\ (1 - \cos 2\theta)\right)$$

so,

$$p_1 = (m_0/\hbar k)\left\{-\hbar\omega_1 + \hbar\omega_2 \left(1 + \left(\hbar\omega_1/m_0c^2\right)\ (1 - \cos 2\theta)\right)\right\}. \tag{31}$$

Since $q \approx p_1$, so

$$\begin{aligned} q &= \frac{(m_0/\hbar)\left\{-\hbar\omega_1 + \hbar\omega_2 \left(1 + \left(\hbar\omega_1/m_0c^2\right)\ (1 - \cos 2\theta)\right)\right\}}{\sqrt{k_1^2 + k_2^2 - 2k_1k_2\ \cos 2\theta}} \\ &= \frac{(m_0c)\left\{-\hbar\omega_1 + \hbar\omega_2 + \left(\hbar^2\omega_1\omega_2/m_0c^2\right)\ (1\ - \cos 2\theta)\right\}}{\sqrt{\hbar^2\omega_1^2 + \hbar^2\omega_2^2 - 2\hbar^2\omega_1\omega_2\ \cos 2\theta}} \end{aligned} \tag{32}$$

Simplifying equation (32), it gives

$$q = \frac{(-137)\left\{\hbar\omega_1 - \hbar\omega_2 - \left(\hbar^2\omega_1\omega_2/m_0c^2\right)\ (1\ - \cos 2\theta)\right\}}{\sqrt{\hbar^2\omega_1^2 + \hbar^2\omega_2^2 - 2\hbar^2\omega_1\omega_2\ \cos 2\theta}} \tag{33}$$

where $m_0c = 137 = 1/\alpha$ and the α is the fine structure constant. Again $m_0c\alpha = \hbar/a_0 = 1$ atomic unit of momentum ($= 1.99275\times10^{-19}$ g $\cdot$ cm/s). In addition, 1a.u. of energy is equal to 27.2 eV. For convenience, the electron momentum can be expressed in energy unit by multiplying it with velocity of light 'c'. So, 1 atomic unit of momentum (in energy unit) = 27.2×137.036 eV = 3.727 keV.

Thus, with the help of this equation (33), the photon spectrum can be transformed to an electron momentum spectrum. The negative sign implies that for positive q values the energy shift is lower. If one assumes k to be along z-direction, then $q = p_{z,}$ so the CP $J(q)$ becomes $J(p_{z,})$.

Simplifying equation (29) as per equation (13), similar to the case of electron in motion, gives

$$\Delta\hbar\omega|_N = (\hbar\omega_3 - \hbar\omega_1) + (\hbar k_p p_1/m_0)$$

or,

$$\hbar\omega_3 = \Delta\hbar\omega|_N + \hbar\omega_1 - (\hbar k_p p_1/m_0). \tag{34}$$

Modifying equation (16) for this scattering gives

$$\Delta\hbar\omega|_N = \left(\hbar^2\omega_1\omega_3/m_0c^2\right)\ (1 - \cos 2\theta'). \tag{35}$$

Simple algebra using equation (34) and (35) leads to the following result:

$$\hbar\omega_3 = \left(\hbar^2\omega_1\omega_3/m_0c^2\right)\ (1 - \cos 2\theta') + \hbar\omega_1 - (\hbar k_p p_1/m_0) \tag{36}$$

Finally, simplifying equation (37), energy of the scattered photon becomes

$$\hbar\omega_3 = \frac{\hbar\ \omega_1}{[1 - \gamma\ (1 - \cos\ 2\theta')]} - \frac{\frac{\hbar}{m}\ k_p p_1}{[1 - \gamma\ (1 - \cos\ 2\theta')]}. \tag{37}$$

Simplifying the value of k_p, using vector diagram shown in Figure 2(b) and applying the first approximation $|k_1|^2 \approx |k_3|^2$ as in equation (15), one can have

$$\begin{aligned} k_p &= \sqrt{(k_3 - k_1)^2} = \sqrt{k_3^2 + k_1^2 - 2k_1k_3\ \cos 2\theta'} \\ &= \sqrt{2k_1^2\,(1 - \cos 2\theta')} = 2\ \left(\frac{\omega_1}{c}\right)\ \sqrt{\sin^2\theta'}. \end{aligned} \tag{38}$$

Hence, the term $\frac{\hbar}{m_0}\ k_p p_1$ in equation (37), as per equation (28), is actually $\frac{\hbar}{m_0}\ k_p p_1'$ and can be simplified to

$$\frac{\hbar}{m_0}\ k_p p_1' = \frac{\hbar}{m_0}\ \left(2\ \left(\frac{\omega_1}{c}\right)\ \sqrt{\sin^2\theta'}\right) \cdot m_0 v' = 2\ \hbar\omega_1 \left(\frac{v'}{c}\right)\ \sqrt{\sin^2\theta'}. \tag{39}$$

Finally, from Equation 37, energy of the newly scattered x-ray photon can be written as

$$\hbar\omega_3 = \frac{\hbar\ \omega_1}{[1 - \gamma\ (1 - \cos\ 2\theta')]} - \frac{\left[2\ \hbar\omega_1\ \left(\frac{v'}{c}\right)\ \sqrt{\sin^2\theta'}\right]}{[1 - \gamma\ (1 - \cos\ 2\theta')]}. \tag{40}$$

This equation (40) is valid for all angles when $\gamma << 1$, i.e., non-relativistic photon (< 15 keV). In this energy range the relativistic effect can be neglected. According to the equation (40), the energy gain by the x-ray photon in this process is of the same order as the amount of energy absorbed in Compton process.

Let us consider q', the plasmons initial state momentum and the new shift associated with the electron oscillation, which may be given as

$$q' = k_p.\ p\ /\ |\,k_p|\,. \tag{41}$$

Hence, q' may be further simplified as,

$$\begin{aligned} q' &= (m_0/\hbar k_p)\left\{\hbar\omega_1 - \hbar\omega_3 + \left(\hbar^2\omega_1\omega_3/m_0c^2\right)\ (1 - \cos 2\theta')\right\} \\ q' &= \frac{(m_0/\hbar)\left\{\hbar\omega_1 - \hbar\omega_3 + \left(\hbar^2\omega_1\omega_3/m_0c^2\right)\ (1 - \cos 2\theta')\right\}}{\sqrt{k_1^2 + k_3^2 - 2k_1k_3\ cos2\theta'}} \\ &= \frac{(m_0c)\left\{\hbar\omega_1 - \hbar\omega_3 + \left(\hbar^2\omega_1\omega_3/m_0c^2\right)\ (1 - \cos 2\theta')\right\}}{\sqrt{\hbar^2\omega_1^2 + \hbar^2\omega_3^2 - 2\hbar^2\omega_1\omega_3\ \cos 2\theta'}}. \end{aligned} \tag{42}$$

Expression (42) gives

$$q' = \frac{(-137)\left\{\hbar\omega_3 - \hbar\omega_1 - \left(\hbar^2\omega_1\omega_3/m_0c^2\right)\ (1\ - \cos 2\theta')\right\}}{\sqrt{\hbar^2\omega_1^2 + \hbar^2\omega_3^2 - 2\hbar^2\omega_1\omega_3\ \cos 2\theta'}}. \tag{43}$$

Thus, with the help of this equation, the photon spectrum can be transferred to an electron momentum spectrum. Thus, q' value will provide vital information to study the new scattering profile, i.e. $J(q')$.

The physical origin of the broadening of the modified line developed by Jauncey [52, 53] and DuMond [54, 55] is known as Compton profile. In that paper, Jauncey pointed out that the interaction between the x-ray photon and the electron in motion gives rise to a second term in the Compton's expression (3), which is dependent on the components of electron's ground state momentum along the scattering vector. The Compton profile (CP), i.e., $J(q)$ is centered around $k^2/2m_0$ with a width $k \cdot p_1/m_0$, where $k = k_1 - k_2$ is the scattering

vector and p_1 is the initial momentum of electron. Therefore, the width of the Compton band [46] can be written as $w_C = 2\ (\lambda\ \lambda')^{1/2}(v/c)\ \sin\theta$. Similarly, when x-ray photon scattered from oscillating electrons (plasmon) gives rise to a second term in equation (9f), which depends on the electron's ground state momentum and the inverse Doppler shift associated with electron in solid-state plasma media. Hence, the new modified profile, i.e., $J(q')$ is centred around $k_p^2/2m_0$ with a width $k_p \cdot p_1/m_0$, where $k_p = k_3 - k_1$ is the scattering vector in solid state plasma media. Similarly, the width of the new modified band in terms of energy can be written, instead of wavelength as,

$$w_N = \frac{\left[2\ \hbar\omega_1\ \left(\frac{v'}{c}\right)\ \sqrt{\sin^2\theta'}\right]}{[1-\gamma\ (1-\cos\ 2\theta')]}.$$

3.4. Intermediate state transition probability

In quantum electrodynamics (QED), a quantized electromagnetic field and free electron interactions involve an initial (ground) state, an intermediate (ionization) state and a final (continuous) state. Momentum and energy are conserved between the initial state and the final state, but in the intermediate state, the theory requires only momentum conservation and not energy conservation. In quantum theory, an external field (if it varies sufficient rapidly) can cause transition from a state of positive energy to state of negative energy [25]. In atomic physics, the ionization level is often assigned the zero energy, and the bound states thus all have negative energies [56]. Hence, the continuum state is assigned positive energy.

As our interest is on scattering of low energy (< 15 keV) x-ray photon, we shall confine ourselves to the non-relativistic (NR) case and its correction to Compton effect. According to the non-relativistic interaction (in Coulomb gauge) between an electron and the radiation field, the Hamiltonian [25, 57] is given by

$$H_{int} = -\frac{e}{m_0c^2}\,(pA) + \frac{e^2}{2m_0c^2}A^2 = H_1 + H_2, \tag{44}$$

where, $\mathbf{A}$ is the vector potential of x-ray field and $\mathbf{p}$ is the momentum operator for the electron.

In case of transition from bound state (or ground state) to continuous state (or final state), i.e., (E_0, k_1) $\rightarrow$ $(E,\ k_3)$, as shown in Figure 3, the perturbation term can be defined as

$$H_1 = -e\sum_k \frac{\alpha_i \cdot e_{k_3}}{\sqrt{2k_1}}\left(a_{k_3}e^{ik_3.x} + a^\dagger_{k_3}\ e^{-ik_3\cdot x}\right), \quad \left[a^\dagger_k = \ a^{-1}\right]. \tag{45}$$

Here, H_1 is a first-order term and α_i is the component of the matrix vector. It can only cause transitions involving two x-ray quanta through the virtual states which differ from the initial and final states by having only one x-ray quantum emitted or absorbed. The free electron wave function for negative energy state, $\psi = u_i(-P_\mu)\ e^{-ipx+iEt}$, where u_i is a spinor function, i is the spin indices and P_μ is a four vector. The H_2 in equation (44) can be given as

$$\begin{aligned} H_2 &= \frac{2\pi\ e^2\hbar^2c^2}{mc^2\sqrt{k_1k_3}}\int \psi^*_n e^{i(k_1-k_3.x)}\ \cdot\ \psi_{n_0}\,(e_{k_1}\cdot e_{k_3}) \\ &= \frac{2\pi\ e^2\hbar^2c^2}{mc^2\sqrt{k_1k_3}}\ e^{i(k_1-k_3.x)}\delta_{n_0\ n}\ (e_{k_1}\cdot e_{k_3})\,, \end{aligned} \tag{46}$$

where $\delta_{n_0\, n}$ is the delta function, e_{k_1}, e_{k_3} denote unit vectors in the direction of polarization of the two quanta k_1, k_3 and the $\mathbf{x}$ denotes a vector specifying the position of the atom.

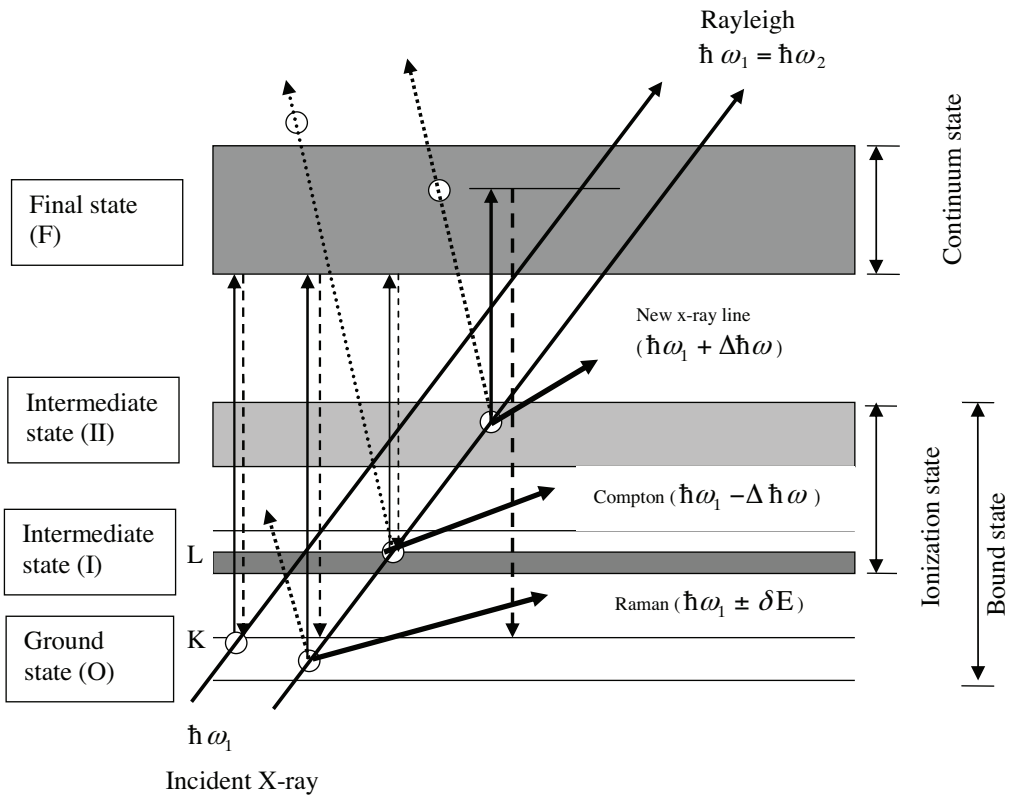

Figure 3. Schematic energy level diagram indicating the mechanism of Compton, Raman and the new incoherent x-ray scattering. This is divided into four sections, the ground state (O) at the bottom of the bound state; the intermediate state (I) of lower energy at the bottom of the ionization state; the intermediate state (II) of higher energy at the top of the ionization state and the final state (F) is the total range of continuum state. As per the transition mechanism, the scattering phenomena are so classified as Rayleigh (between top of the ground state to bottom of the continuum state), Raman (between bottom of the ground state to bottom of the continuum state), Compton (between lower ionization state, *i.e.*, intermediate state (I) and bottom of the continuum state) and the new incoherent scattering (between higher ionization state, i.e., intermediate state (II) and top of the continuum state).

Denoting the Dirac's amplitudes of the electron with the momenta p_0, p, p', p'' by u_0, u, u', u'', respectively, and the α_i in the direction of polarization of the two x-ray quanta k_1 and k_3 simply by α_1 and α_3, respectively, the matrix M occurring in the transition probability (F$\rightarrow$ O) is formulated as

$$\begin{aligned} M &= \sum \left(\frac{H_{OI} H_{IF}}{E_I - E_O} + \frac{H_{OII} H_{IIF}}{E_{II} - E_O} \right) \\ &= \sum_{n'} \frac{(i\,|H_1|\,n')\ (n'\,|H_1|\,f)}{E_I - E_O} + \sum_{n''} \frac{(i\,|H_1|\,n'')\ (n''\,|H_1|\,f)}{E_{II} - E_O} \\ &= \sum_{n'} \frac{(u^* \alpha_3\, u')\ (u'^* \alpha_1\, u_0)}{E_I - E_O} + \sum_{n''} \frac{(u^* \alpha_3\, u'')\ (u''^* \alpha_1\, u_0)}{E_{II} - E_O}, \end{aligned} \tag{47}$$

where the summations are over the four intermediate states including both signs of the energy ($\pm E$) and both sign of the spin ($\uparrow\downarrow$). E_i is the energy of initial state and E'_n, E''_n are the energies of the two types of intermediate state. E_O, E_I, and E_{II} denote the total energies in the initial and intermediate states. For calculation of the transition probability from the final state F(k_3, $p_3 \neq 0$) to the initial state O(k_1, $p_1 = 0$), assuming that the process can happen only by passing through an intermediate state which can differ by one quantum ($\hbar\omega$) only from O or F, the respective Hamiltonian [25], can be expressed as

$$H_{IF} = (n' \,|H_1\,| f) \;= -e\sqrt{\frac{2\pi\,\hbar^2 c^2}{k_3}} \quad (u'^{*}\alpha_3\, u)\,, \tag{48a}$$

$$H_{OI} = (i \,|H_1\,| n') \;= -e\sqrt{\frac{2\pi\,\hbar^2 c^2}{k_1}} \quad (u_1^{*}\alpha_1\, u')\,, \tag{48b}$$

$$H_{IIF} = (n'' \,|H_1\,| f) \;= -e\sqrt{\frac{2\pi\,\hbar^2 c^2}{k_1}} \quad (u''^{*}\alpha_1\, u)\,, \tag{48c}$$

$$H_{OII} = (i \,|H_1\,| n'') \;= -e\sqrt{\frac{2\pi\,\hbar^2 c^2}{k_3}} \quad (u_1^{*}\alpha_3\, u'')\,. \tag{48d}$$

Only the momentum and not the energy is conserved in these intermediate or virtual states. Hence, the energy difference can be formulated as

$$E_I - E_O = E' - \left(m_0c^2 + k_1\right) \tag{49}$$

$$\begin{aligned} E_{II} - E_O &= (E'' + k_1 + k_3) - \left(m_0c^2 + k_1\right) \\ &= (E'' + k_3) - m_0c^2. \end{aligned} \tag{50}$$

The transition probability per unit time for the new scattering process can be defined as

$$w = \frac{2\pi}{\hbar}\;|M|^2\,\rho_F, \tag{51}$$

where ρ_F denotes the number of final states per energy interval dE_F. Since the final energy is given as a function of k_3 and θ', one can have

$$E_F = k_3 + \sqrt{k_p^2 + (m_0c^2)}^2 \tag{52}$$

$$k_p^2 = k_1^2 + k_3^2 - 2k_1k_3\cos 2\theta'. \tag{53}$$

Thus, $\left(\frac{dk}{dE_F}\right)_\theta = \frac{E\,k_3}{k_1 \cdot m_0 c^2}$, where E is the electron energy in the final state and

$$\rho_F = \rho_k \left(\frac{dk}{dE_F}\right)_\theta \qquad [\rho_F \cdot dE_F = \rho_k \cdot dk]$$

$$\rho_F = \frac{d\Omega\; k_3^2}{(2\pi\;\hbar\;c)^3}\;\frac{E\;k_3}{k_1 \cdot m_0 c^2} \tag{54}$$

where $d\Omega = 2\pi\;\sin\theta\;d\theta$, is the element of solid angle for the scattered quanta.

Applying equation (49) and (50) in the equation (47), one can have

$$\begin{aligned} M &= \sum_{n'} \frac{\left(u^* \alpha\, u'\right)\left(u'^* \alpha_0\, u_0\right)}{E' - (m_0c^2 + k_1)} + \sum_{n''} \frac{\left(u^* \alpha\, u''\right)\left(u''^* \alpha_0\, u_0\right)}{(E'' + k_3) - m_0c^2} \\ &= M_1 + M_2 \end{aligned} \tag{55}$$

As defined by Heitler [25], simplifying the differential cross section for this scattering of the photon into the momentum state k_3, we have

$$d\sigma = \frac{e^4\ E\ k_3^2}{k_1^2 \cdot m_0c^2} \left|M\right|^2\ d\Omega. \tag{56}$$

On rearranging equation (56), it becomes

$$\frac{d\sigma}{d\Omega} = \left(\frac{k_3^2}{k_1^2}\right)\left(\frac{E}{m_0c^2}\right)\ e^4 \left|M\right|^2. \tag{57}$$

This result is valid for a given polarization of both quanta and a given spin direction of the electron in the initial and final states. The summations in equation (55) are over all spin directions and both signs of the energy for the intermediate states. Hence, the energy denominators of M are different for the positive energy and negative energy state.

Further simplifying, the above equation (57), one can have

$$\frac{d\sigma}{d\Omega} = \left(\frac{e^2}{m_0c^2}\right)^2 \left(\frac{k_3^2}{k_1^2}\right)\left(E\ m_0c^2\right)\ \left|M\right|^2, \tag{58}$$

where $\frac{e^2}{m_0c^2}$ $(= r_0)$ has the dimension of length, the so-called "classical electron radius" and is equal to 2.82×10^{-13}cm. Hence,

$$\frac{d\sigma}{d\Omega} = (r_o)^2\ \left(\frac{k_3^2}{k_1^2}\right)\left(E\ m_0c^2\right)\ \left|M\right|^2 \tag{59}$$

or,

$$\frac{d\sigma}{d\Omega} = (\sigma_T)\ \left(\frac{k_3^2}{k_1^2}\right)\left(\frac{3\ E\ m_0c^2}{8\pi}\right)\ \left|M\right|^2 \tag{60}$$

whereσ_T $(= 6.65 \times 10^{-25}\,\mathrm{cm}^2/\text{electron})$ is known as the Thompson scattering cross section. The deduction of QED cross section can be done with the evaluation of the matrix M in equation (60) (see Appendix-A for derivation). The derivation of the cross section, which ends up with equation (58), is based solely on the $\mathbf{p} \cdot \mathbf{A}$ term of the interaction Hamiltonian. As mentioned in Ohmura and Matsudaira [58], in the x-ray plasmon scattering the term $\mathbf{p} \cdot \mathbf{A}$ is negligible in Compton cross section for all possible practical scattering angles [59]. Hence, the contribution of the $\mathbf{A}^2$ term of the interacting Hamiltonian to the x-ray Compton cross section is the prime interest here. Therefore, the scattering cross section (based solely on the $\mathbf{A}^2$ term) was derived applying statistical approach described below.

3.5. Scattering cross section

In the statistical model of the atom, incoherent scattering cross section of x-rays by a system of interacting particles is expressible in terms of density distribution functions for the system [60, 61] as

$$\sigma(k) = \sigma_T \int P(k,r)\, n(r)\, dr, \tag{61}$$

where $P(k,r)$ is the local correlation function, and $n(r)$ is the electron density function.

However, the maximum information about the many-particle system is contained in the quantity $P(k,\omega)$, which is the Fourier transformation in space and time of the time-dependent pair-distribution function for the system [60–63] and is also known as spectral function. The spectral function $P(k,\omega)$ is directly measured in an inelastic-scattering experiment. Applying the Born approximation, one can find the angular and energy distribution of scattered photon as

$$\frac{d^2\sigma}{d\Omega\, d\omega} = \frac{m_0^2}{8\pi^3}\frac{p_3}{p_2}\, V_k^2\; P(k,\omega) \tag{62}$$

for the particle (electron) of mass m_0, initial momentum p_2 scattered to a final momentum p_3, with energy transfer between ω and $\omega + d\omega$, and scattering angle specified by $d\Omega$. The energy transfer $\Delta\hbar\omega|_N$ is related to the momentum transfer and scattering angle as given in expression (29). In the case of collective mode, the Coulomb interaction factor V_k [62] is simplified as

$$V_k = 4\pi\, e^2/k_p^2. \tag{63}$$

However, the static Coulomb interaction generated due to the scalar field (static field) $\phi\,(r,t)$, a well-defined function of the particle coordinates at the same time [25].

Again, this $P(k,\omega)$ is related to the structure factor $P(k)$ [62] by

$$\int_{-\infty}^{\infty} P(k,\omega)\, d\omega = \; P(k)\, n_e \tag{64}$$

where, $P(k) = \left\langle \psi_o \;\middle|\rho_k^\dagger \rho_k\middle|\; \psi_o \right\rangle / n_e$, and the $P(k)$ is directly measured in a scattering experiment in which one determines the differential cross section. Then the differential cross section is determined by integrating over all energy transfers [62]:

$$\frac{d\sigma}{d\theta'} = \int_0^{\infty} \frac{d^2\sigma}{d\theta\, d\omega}\, d\omega = \frac{m_0^2}{8\pi^3}\frac{p_3}{p_1}\, V_k^2\; P(k)\, n_e. \tag{65}$$

For the evaluation of the incoherent form factor by applying non-interacting Fermi gas models of the atom such as Thomas-Fermi (TF) and Thomas-Fermi-Dirac (TFD) fails to explain in this system. The deficiencies of the above models can be removed by introducing the correlations brought about by the electrostatic interaction between electrons, i.e., considering the interacting Fermi gas [61]. As described, the interacting Fermi gas model deals with relation between the pair distribution function and the dielectric constant of the uniform gas [61, 64]. In the interacting Fermi gas model, the correlation term $P(k,r)$ used in the above equation (61) can be taken as $P(k)$ (for brevity by omitting the argument r) and can be expressed in the random-phase approximation

(RPA) as a function of dielectric constant $\in (k,\omega)$ as

$$P(k) = \frac{\hbar\, k_p^2}{4\pi^2\, n_e\, e^2} \int_0^\infty \frac{\in_2 (k,\omega)}{|\in (k,\omega)|^2}\, d\omega \tag{66}$$

where, $\in (k,\omega) = \in_1 (k,\omega) + i \in_2 (k,\omega)$.

After a bit of algebraic simplification, one can have the $P(k)$ as the same as given in earlier expression (64).

The various physical phenomena existing within the concept of incoherent x-ray scattering can be classified in three meaningful catagories according to the associated energy transfer $\Delta\hbar\omega$ (expression (21)) and momentum transfer k (expression (15)) in relation to the characteristic energies or structural dimensions. The above three distinct regimes are: the Compton scattering regime ($\Delta\hbar\omega >> E_B,\ k\ r_{nl} >> 1$), i.e., the energy (momentum) transfer is large compared to the binding energy E_B(inverse of the orbital radiusr_{nl}) of the target electron; the characteristics excitation (Raman scattering) regime ($\Delta\hbar\omega \cong E_B,\ k\ r_{nl} \cong 1$), i.e., the energy (momentum) transfer is comparable to the E_B (inverse of the r_{nl} or inter atomic distance) of the target system; and the collective scattering regime ($\Delta\hbar\omega << 1\ keV,\ k\ r_{nl} << 1$), i.e., the energy (momentum) transfer is very small (< 1 keV) compared to E_B (inverse of inter atomic distance) of the target material [65]. The excitation may be either of local or collective type. In a uniform gas, for small values of the wave number k_p, there are two kinds of excitation contributions to $P(k)$; one is the particle-hole pair excitations and the other one is the collective excitations [61, 62]. For electron gas, the collective mode is the plasmon. A quantized plasmon oscillation correspond to oscillations in the particle density. The collective contribution to$P(k)$ in the small k_p region is, to an accuracy k_p^4/k_{TF}^4,

$$P_{coll}(k) = \frac{\hbar^2\, k_p^2}{2m\, \omega_k}, \tag{67}$$

where ω_k is the oscillation frequency of the collective mode with the wave number k_p and k_{TF} is the Thomas-Fermi screening wave number, $k_{TF}^2 = (4/\pi)(k_F/a_0)$, and a_0 is the Bohr radius [62].

The dielectric function $\varepsilon(\omega,k)$ of the electron gas is strongly dependent on the frequency and wavevector. A number of theories or models related to $\varepsilon(\omega,k)$ has been given [63]. Due of the complexity of the many body problem, knowledge of the exact dielectric function is still lacking. However, we are interested, here, in RPA type dielectric function. The RPA is also called the Lindhard dielectric function and is a model for a static $\varepsilon(k)$ or dynamic $\varepsilon(\omega,k)$ dielectric function [63]. For brevity, we do not exhibit here the frequency dependence (the predicted scattering is highly dependent on critical number density of plasom n_c).

According to the dispersion relation, the collective frequency ω_k of the electromagnetic wave propagated in solid [50] can be simplified as

$$\omega_k = \left[\frac{c^2 k_p^2}{\varepsilon(\omega,k)}\right]^{\frac{1}{2}} = \left[\frac{4\pi\, c^2 k_p^2}{\in}\right]^{\frac{1}{2}} \tag{68}$$

As it is already mentioned earlier, $\varepsilon\ = \varepsilon_0\ \in$, and $\varepsilon_0\ = 1/4\pi$ (see the hypothesis, i.e., section 2). Also, using equation (4),

$$\omega_k = \left[\frac{c^2 k_p^2}{(n_c - n_e)/n_c}\right]^{\frac{1}{2}}. \tag{69}$$

Hence, simplifying equation (65) using expressions (63) and (67), one can have

$$\begin{aligned}
\frac{d\sigma}{d\theta'} &= \frac{m_0^2}{8\pi^3}\frac{p_3}{p_2}\left(\frac{4\pi\, e^2}{k_p^2}\right)^2 \frac{\hbar^2\, k_p^2}{2m_0\, \omega_k}\, n_e \\
&= \frac{m_0^2}{8\pi^3}\frac{p_3}{p_2}\left(\frac{4\pi\, e^2}{k_p^2}\right)^2 \frac{\hbar^2\, k_p^2}{2m_0}\left[\frac{\in}{4\pi\, c^2 k_p^2}\right]^{\frac{1}{2}} n_e [\text{substituting } \omega_k \text{ from (68)}] \qquad (70) \\
&= \left(\frac{e^2}{m_0 c^2}\right)^2 \left(\frac{1}{k_p}\right)^3 \frac{(m_0 c)^4}{16\pi^3}\frac{p_3}{p_2}\,\frac{\hbar^2}{(m_0 c)}\,[4\pi]^{\frac{3}{2}}\,[\in]^{\frac{1}{2}}\, n_e \\
&= (r_0)^2 \left(\frac{1}{k_p}\right)^3 \left[\frac{(m_0 c)^3 \hbar^2 (4\pi)^{\frac{3}{2}}}{16\pi^3}\right]\frac{p_3}{p_2}\,[\in]^{\frac{1}{2}}\, n_e \\
&= \frac{8\pi}{3}(r_0)^2 \left(\frac{1}{k_p}\right)^3 \left[\frac{(137)^3 \hbar^2 (4\pi)^{\frac{3}{2}}}{16\pi^3 \times \frac{8\pi}{3}}\right]\frac{p_3}{p_2}\,[\in]^{\frac{1}{2}}\, n_e \\
&= \sigma_T \left(\frac{1}{k_p}\right)^3 \left[\frac{(137)^3\, \hbar^2}{\pi^{\frac{5}{2}} \times \frac{16}{3}}\right]\frac{p_3}{p_2}\,[\in]^{\frac{1}{2}}\, n_e. \qquad (71)
\end{aligned}$$

Hence,

$$\frac{d\sigma}{d\theta'} = \sigma_T \left(\frac{1}{k_p}\right)^3 M_c \frac{p_3}{p_2}\,(\in)^{\frac{1}{2}} n_e, \qquad (72)$$

where M_c ($\approx 2.756 \times 10^4$) is a constant quantity, since, $m_0 c = 137$ and considering $\hbar = c = 1$, as used to study x-ray scattering from electron gas [17, 18]. Since the solid angle $\Omega(r, \theta')$ is a function of r and θ', the above equation (72) can be written as

$$\left(\frac{d\sigma}{d\Omega}\right)_N = \sigma_T \left(\frac{1}{k_p}\right)^3 M_c \frac{p_3}{p_2}\,(\in)^{\frac{1}{2}} n_e \qquad (73)$$

However, $\left(\frac{d\sigma}{d\Omega}\right)$ over this plasmon line is already defined in DuBois and Gilinsky [14].

The total cross section of this new incoherent scattering can be obtained by integrating the equation (73) over the solid angle, $d\Omega = 2\pi\, \sin\theta'\, d\theta'$:

$$\sigma_N = \int \left(\frac{d\sigma}{d\Omega}\right)_N d\Omega \qquad (74)$$

or,

$$\sigma_N = \sigma_T \left(\frac{1}{k_p}\right)^3 M_c \frac{p_3}{p_2}\,(\in)^{\frac{1}{2}} n_e \int_0^{\pi} 2\pi\, \sin\theta'\, d\theta'. \qquad (75)$$

Finally, the total scattering cross section of this new scattering is found out to be

$$\sigma_N = \sigma_T \left(\frac{1}{k_p}\right)^3 M_c \frac{p_3}{p_2}\,(\in)^{\frac{1}{2}} n_e\,(4\pi), \qquad (76)$$

where the scattering vector k_p has magnitude $k_p = (4\pi/\lambda'')\, \sin\theta'$. Hence, the new scattering cross section is found out to be inversely proportional to the third power of momentum transfer, i.e., k_p^{-3}. In addition, this new

scattering cross section is found out to be directly proportional to the $\sqrt{\in}$ as predicted in the hypothesis. Also the final momentum p_3 or the momentum of the relaxed electron after scattering of the photon of enhanced energy is the same as the initial momentum p_1, i.e. $p_3 \approx p_1$.

Further simplified, alternative form of the total scattering cross section of this new scattering is found out to be

$$\sigma_N = \sigma_T \left(\frac{1}{k_p}\right)^3 M_c' \frac{p_3}{p_2} \left(\left| \frac{n_c - n_e}{n_c} \right| \right)^{\frac{1}{2}} n_e, \tag{77}$$

where M_c' $(= (4\pi)^{\frac{3}{2}} M_c)$ is a constant.

3.6. Scattering intensity

The scattered intensity is described by the double differential cross section $\frac{d^2\sigma}{d\Omega\, d\omega}$, and the inelastic scattering intensity includes both contributions of the coherent and the incoherent parts. Physical concepts behind both the scattering parts and their respective functions are given elsewhere [66, 67]. Theoretical calculation of the intensity of scattering of x-rays by recoiling electrons is defined by Woo [68]. However, for the experimental intensity of inelastic scattering as observed by Paakkari and Suortti [69] for the symmetrical-reflection geometry, i.e., the incident and detected rays making equal angle θ with the flat specimen surface, the expression is modified because of this new type incoherent scattering to

$$I = I_O\ \Omega\ M_O\ K_{pol} \left(\frac{(d\sigma/d\Omega)_C}{\mu_O + \mu_C} + \frac{(d\sigma/d\Omega)_{TDS}}{2\mu_O} + \frac{(d\sigma/d\Omega)_N}{\mu_O + \mu_N} \right), \tag{78}$$

where I is the intensity of the inelastic scattering, I_O is the intensity of the primary beam, Ω is the solid angle subtended by the receiving slit, M_O is the number of atoms per unit volume and K_{pol} is the ratio of the polarization factor of the scattered radiation to that of the monochromatic primary beam. In the present case, this can be written [69] as

$$K_{pol} = \frac{(1 + K' \cos^2 2\theta')}{(1 + K')} \tag{79}$$

where K' $(= I(\pi)/I(\sigma))$ is the polarization ratio of the primary beam.

Again, in the above equation (79), the linear absorption coefficients for the unmodified, Compton-modified and modified by this new incoherent process are denoted by μ_O, μ_C and μ_N, respectively. Also, the scattering cross sections per atom are: for the Compton process C, $(d\sigma/d\Omega)_C$, for the thermal diffusion scattering *TDS*, $(d\sigma/d\Omega)_{TDS}$, and for the new incoherent scattering process, $(d\sigma/d\Omega)_N$. This new scattering cross section has been derived in the earlier section (3.5) of this paper in equation (74). However, the other two scattering cross sections have already been reported by others elsewhere [69].

4. Experimental

X-ray scattering experiments have been carried out using two types of x-ray instruments, i.e., wavelength dispersive x-ray (WDXR) spectrometry [70] and energy dispersive x-ray fluorescence (WDXR and EDXRF) spectrometry [71, 72] techniques for spectroscopic analysis of materials. The details of the WDXR, EDXRF spectrometry techniques are discussed below.

4.1. Wavelength dispersive x-ray spectrometry

A WDXR spectrometer (Philips analytical x-ray instrument, Model No.-PW 3020, Netherlands) employing Bragg-Brentano parafocusing optics with an energy resolution $\frac{\Delta E}{E} = 1 \times 10^{-3}$ was used for the scattering study. The system shows the FWHM of 8 eV at 8 keV x-ray, which corresponds to a momentum resolution of about 0.16 a.u., calculated using the relations given in references [73–75].

A section was examined via the scattering geometry shown in Figure 4(a). Incident line focus came from CuK_α or CoK_α radiation produced by a high-power ceramic tube of focus dimension 12 mm $\times$ 0.4 mm, operated at 40 kV and 40 mA using a 2.0 kW (40 kV and 50 mA) x-ray generator. Radiation was passed through a Be window having 93% transmission, emitting CuK_α x-ray (1.289×10^{-15} J) photons on the order of 1.2×10^{16} photon/s ($= \frac{1600\,W \times 0.93 \times 0.01}{1.289 \times 10^{-15} J}$, with only 1% of power converted to CuK_α x-ray, which can be achieved using modern high-power ceramic tube). Monochromatic photons of the order of 10^9 photon/s can be obtained using a presently available high-power sealed-off tube [75]. The CuK_α excitation from the line focus tube was filtered by a β-filter, then the x-ray beam was collimated through Soller slit (SS) of 0.04 rad., fixed divergence slit (FDS) of 2° and mask (10 mm) before irradiating the sample. The scattered x-ray beam from the sample was well collimated by passing it through a programmable anti-scattering slit (PASS) of 2° (to reduce air scattering), programmable receiving slit (PRS) of 0.8 mm and Soller slit (SS) of 0.04 rad. before getting it reflected by the Johannson-type curved graphite crystal (002) monochromator of radius 225 mm. The monochromator crystal has an interplaner spacing is 3.383 Å. The graphite monochromator gives an intensity gain of about 70 in comparison with silicon crystals in the same geometry [76]. Since x-ray absorption depends approximately on Z^4, while maximum possible diffraction power is proportional to Z^2 (mosaic crystal case), where Z is the atomic number, the crystals of the lighter elements are expected to form better monochromators then those of heavier elements [2, 77]. A sophisticated Xe-gas filled proportional counter (PW 3011) having 8 mm $\times$ 26 mm window size and 19% energy resolution was mounted on the arm of the goniometer circle of radius 200 mm. The counter is capable to possess maximum count rate of 750 kcps with a background of 2 cps. Step size chosen for this experiment was 1°. In this arrangement, x-rays are reflected from both the specimen and the focusing monochromator, which is known as reflection-reflection mode in double-crystal spectrometry (+ -) [2]. Data have been collected in an absolute-scan mode (scanning 2θ and keeping sample fixed with respect to the beam direction). Experimental set up was fully computer-controlled. The observed spectra were fitted using X'Pert Graphics software supplied by Philips, Netherlands [78].

4.2. Energy dispersive x-ray spectrometry

Samples were also characterized via Energy Dispersive X-ray Fluorescence (EDXRF) using an Oxford model XTF-5020/W triple-axis EDXRF spectrometer as shown in Figure 4(b). Power supply unit used is the SPELLMAN, USA (50 kV/2.0 mA) air-cool unit. The experiment was performed on powder and crystals using MoK_β and PbL_α x-rays as a secondary radiation from a tungsten anode based x-ray tube operated at 40 kV and 1 mA. The crystal was mounted in such a way that scattered radiation was received by the Canberra, USA make Si (Li) detector (Model no. SL30160) set at 90° and 125° with respect to the incident beam. The detector head is placed at a distance of 30 mm from the sample surface. The scattered beam consisting of coherent, incoherent components and fluorescence is directly counted by a 3 mm thick Si(Li) crystal. The

detector is biased with negative 500 V using a Canberra make HV power supply unit (Model 3106D). The Si(Li) detector having an 8 μm thick beryllium window with a resolution of 180 eV (FWHM) at 5.9 keV x-ray with a momentum resolution about 0.39 a.u at a back scattered geometry, calculated using the relations given in the references [74, 75, 79]. The detector signal was further amplified (shaping time 2 μs) using an ORTEC 572A amplifier mounted in an ORTEC BIN (Model No. 4001C). This amplified signal was fed into an automated PC-based multi-channel analyzer (MCA) for recording the data. The peak area was set at a suitable range of 1–2 K to register the total spectrum [80]. The peak areas of each spectrum were evaluated by least squares fitting method using the AXIL program [81] supplied by International Atomic Energy Agency (IAEA).

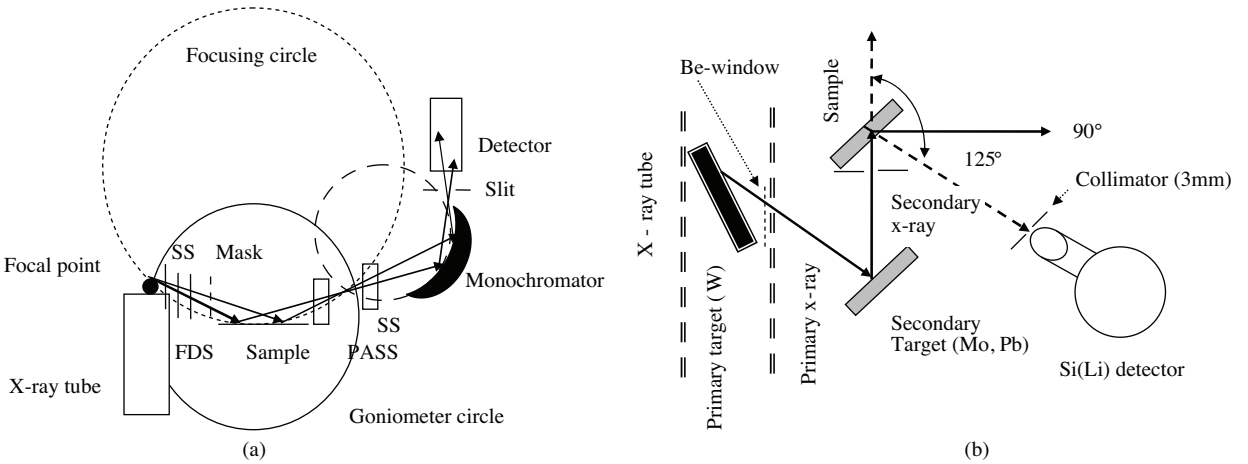

Figure 4. (a) Geometry of the wavelength-dispersive x-ray (WDXR) spectrometry having Bragg-Brentano parafocusing optics (the abbreviations used are. SS for solar slit, FDS for fixed divergence slit, PASS for programmable anti-scattering slit, PRS for programmable receiving slit), and (b) geometry of triple axis energy-dispersive x-ray fluorescence (EDXRF) spectrometry.

5. Results and discussion

Compton scattering studies were carried out using photons of energy on the order of $\times 10^2$ keV, having scattering cross section of the order of 10^{-25} cm^2/electron. This can be calculated using the well-known expression for the cross section [25, 82]:

$$\sigma_C = \sigma_T \frac{3}{4} \left\{ \frac{1+\gamma}{\gamma^3} \left[\frac{2\gamma\ (1+\gamma)}{(1+2\gamma)} - \ln\ (1+2\gamma) \right] + \frac{\ln\ (1+2\gamma)}{2\gamma} - \frac{(1+3\gamma)}{(1+2\gamma)^2} \right\}.$$

At the same time the total scattering cross section of this new scattering, i.e. σ_N, derived in equation (76) and calculated to be of the order of 10^{-27} cm^2/electron, is nearly 100 times less than the σ_C. This is one of the vital reasons for the non observance of this type of incoherent scattering peak in the earlier Compton scattering experiments. However, experimentally it seems feasible to observe this kind of scattering phenomenon using low-energy x-ray photon. For photons of energy about 10 keV ($\gamma << 1$), the energy (maximum) absorbed by the excited (recoil) electron is of the order of 400 eV for scattering in the backward direction. The energy absorbed by the excited (recoil) electron is a function of the scattering angle as given in equation (16). Usually,

Thompson scattering (coherent) cross section σ_T is of the order of 10^{-24} cm^2/electron. Since a non-relativistic (NR) description of incoherent scattering can be applied to x-rays below roughly 15 keV [83], in this energy range, the relativistic effects are negligible. Therefore, NR treatment can be applied to analyze this new scattering cross section.

The Compton cross section is of the same order as the Thompson cross section, i.e., $\sigma_C = 10^{-24}$ cm^2/electron in NR region [25]. In the Compton process, the total scattering cross section for 10 keV x-rays is of the order of 10^{-24} cm^2/electron. However, the σ_N is of the order of 10^{-23} cm^2/electron, which is nearly 10 times greater than the Compton cross section in NR region. This is calculated by taking the lowest value of the momentum (velocity) ratio of electron, i.e., $\frac{p_3}{p_2}$ as 0.1. Since velocity ratio $\frac{v_3}{v_2} = \frac{10^6}{10^7} \approx 0.1$, the maximum velocity attained by the excited electron (plasmon or recoil) v_2 due to Compton process is nearly of the order of 10^7 m/s or less and after transferring this energy the excited electron attains a relaxed velocity v_3, which is same as the orbital velocity v_1 and is of the order of 10^6 m/s. In actual practice, the v_2 is quite low hence the above velocity (or momentum) ratio is high, so a high value of scattering cross section can be observed. Again, the lifetime of plasmon excitation and the incident photon flux, which are very sensitive and bear out the idea of feasibility of this new type of scattering phenomena. The lifetime of the plasmon excitation is of the order of 10^{-16} s [84, 85], at the same time the lifecycle of the plasmon standing wave generated due to Compton effect (using low energy x-ray of 10 keV) calculated using de Brogile's hypothesis is of the order of 10^{-16} s. Since, the number of photon emitted by the source is of the order of 10^{16} photon/s (as calculated in Experimental section 4.1), the possibility of this type of collision cannot be ignore. Hence, it is positive to think the experimental feasibility of such type of x-ray scattering from the plasmon standing wave whose lifecycle is few hundred times greater than the previous one (x-ray wave).

Further, the $\sqrt{\in}$ term leads to a high value of scattering cross section from materials of high dielectric constant. As discussed, for low energy (10 keV) photons, σ_N is on the order of 10^{-23} cm^2 per unit solid angle, and since there are roughly 10^{22} electrons (scatterers) per unit volume, one would expect one part in 10 of the incident beam to be scattered per cm^3 of sample into a unit solid angle. Observation of higher order of magnitude of the scattering cross section is justified, since our interest is on scattering of x-ray from materials of negative refractive index (virtual), where, $n_c < n_e$. Since, the experimental scattering cross section depends on both photon flux density (I_0) at target and number density of electron (n_e), i.e., $\left(\frac{d\sigma}{d\Omega}\right)_C = \frac{Y_{corr}}{(d\Omega)_D\ n_e\ I_0}$ where, Y_{corr} is the corrected yield (see Appendix-B) and $(d\Omega)_D$ is the detector solid angle [48]. So, with our assumption (materials of negative refractive index, $n_c < n_e$) the new scattering cross section may be given as $\left(\frac{d\sigma}{d\Omega}\right)_N = \frac{Y_{corr}}{(d\Omega)_D\ n_c\ I_0}$, when n_c is the critical plasmon density where $n_c < n_e$.

Experimental existence of very low magnitude of scattering cross section such as in high-energy gamma-ray Compton scattering (10^{-26}cm^2/sr.) [48], x-ray Raman scattering (10^{-29}cm^2/sr.) [9, 86, 87] and proton Compton scattering (10^{-32}cm^2/sr.) [33] has already been reported by various researchers. At the same time, electron Compton scattering cross section higher by five orders of magnitude has been reported [30].

In order to ascertain that the new modified x-ray line observed is not accidental or random one, experiments have been performed on different samples since 2000, using different x-ray wavelengths in both energy- and wavelength-dispersive spectrometers [43]. It was found that the existence of this new peak was as real and reproducible as the Compton peak and was highly dependent upon scattering angle and characteristics of the scattering substances.

5.1. WDXR spectral analysis

As discussed in the instrumental section, CoK_α and CuK_α x-ray signals are detected using a Xe-filled proportional counter. Therefore, there is possibility to detect an extra peak in the patterns observed using x-ray (Co and Cu) radiations and Xe-filled proportional counter, since CoK_α (6.92 keV) and CuK_α (8.04 keV) are both energetic enough to excite XeL_α (absorption edge energy 4.78 keV) and emit 4.14 keV energetic line spectra. Therefore, the spectra will contain CoK_α and CuK_α escape peaks in the respective x-ray spectrogram. The energy of these escape peaks will be simply the difference between the energy of XeL_α and CoK_α or CuK_α, respectively. However, the escape of CoK_α (6.92–4.14) and CuK_α (8.04–4.14) arise at 2.78 keV and 3.90 keV, respectively, in the respective spectra. This well-separated keV energy peak from its incident x-ray peak arises on the low-energy side (high-angle side in WDXR spectra) after the Compton tail and can be easily identified, since the largest energy transfer in the Compton collision process is only a few hundred eV. Therefore, the new incoherent scattered peak can be well separated from the escape or spurious peak.

5.1.1. Solid PET

The organic substances are typically made up of many hydrocarbons and pose extremely difficult problem to determine the scattering factors in these condensed states, since the interference effects between molecules would be difficult to separate from the molecular structure factors. However, the Compton profile provides a method for determining the accuracy of wave functions, since there are no comparable interference effects [2, 88]. Again, these condensed states consist of low-Z elements, so the binding energy is less. Therefore, the condensed state of hydrocarbons like polymers offers opportunity to study the Compton effect by researchers. A number of works on the Compton effect in polymers have been reported [33, 40, 89–91].

The scattered spectra of CoK_α (6.923 keV) x-rays by a 3 mm thick and 15×25 mm^2 area polyethylene terephthalate ($[C_{10}H_8O_4]_n$) or PET target using WDXR spectrometry are shown in Figures 5(a) and (b). With an exposure of 10 h at 40 kV and 30 mA, at scattering angle 109.5^o (2θ), the spectra possess usual coherent, incoherent (Compton) peaks with a new x-ray incoherent peak at the low-angle (high-energy) side of the spectrogram. The total spectrum was collected with a scan speed of 0.00075 degree/s. The raw or smeared

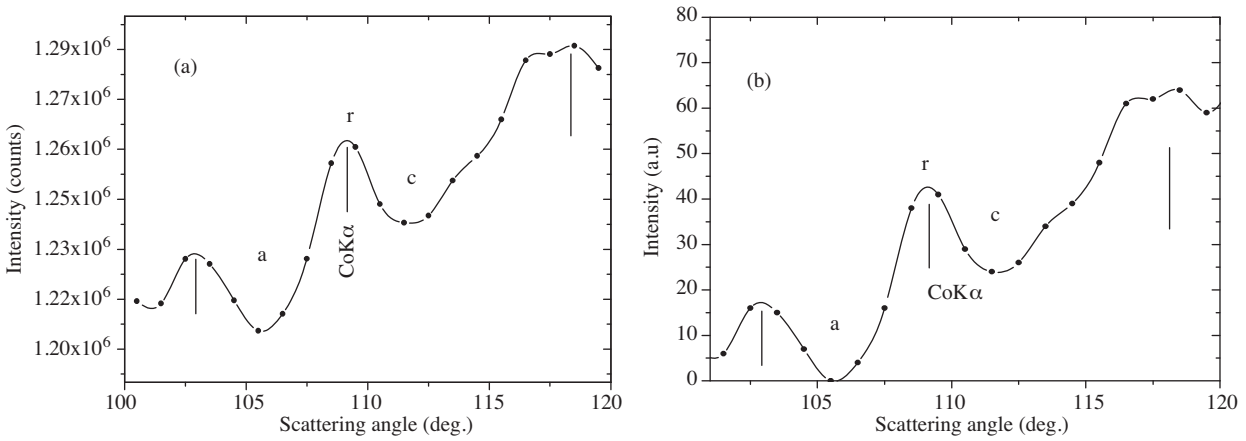

Figure 5. (a) WDXR scattering spectra (accumulation of 10 h) of smeared intensity data obtained from PET solid at 109.5° using CoK_α X-radiation, and (b) the de-smeared data of the x-ray spectra showing unmodified line ($\boldsymbol{r}$), Compton ($\boldsymbol{c}$) and the new incoherent scattering ($\boldsymbol{a}$) peak.

intensity was of the order of 10^6 scattered photons and is shown in Figure 5(a). However, the de-smeared data, i.e., after subtracting background is shown in Figure 5(b). The wavelength shift of the Compton peak, which varies with the scattering angle 2θ (109.5^o), was calculated to be about 0.0327 Å and is given in Table 1.

Table 1. X-ray scattered- profile data for solid PET $CoK_{\alpha 1}$ applying WDXR spectrometry.

Parameter	Experimental value	Parameter	Experimental value
γ	0.014	$\in$	3.4
2θ / °	109.5	n (6)	±0.52
v/c^a	0.048	Z^b_{eff}	6.64
λ / Å	1.79591	$n^c_e/10^{22}$ e/cm^3	2.91
$\hbar\omega_1$/ keV	6.923	E^d_p /eV	18.77
$\hbar\omega_2$/ keV (24)	6.874	E^e_B /eV	13.6 (H 1s) 286 (C 1s)
$\hbar\omega_3$/ keV (40)	7.008	I_a /I_r	0.394
$q/a.u$ (33)	+0.952	I_c /I_r	1.479
q'/ $a.u$ (43)	+0.454	I_a /R_c	12.17
$\Delta\lambda_c$/Å (25)	0.0327 ± 0.0002 (E) 0.0324 ± 0.0001 (T)	k_p /Å $^{-1}$ (76)	5.71 ± 0.02 (E) 5.81 ± 0.01 (T)
$\Delta\lambda_N$/Å (10)	0.0320 ± 0.0002 (E) 0.0324 ± 0.0002 (T)	$\sigma_N/10^{-24}$ (76) cm^2/electron	44.88 ± 2.76 (E) 42.50 ± 2.43 (T)

[a] Using the relation $\frac{v}{c} = \frac{1}{137.0377} Z_{eff}$ [F. K. Richtmyer, E. H. Kennard, and J. N. Cooper, *Introduction to Modern Physics*, 6th Ed., p. 236, Tata McGraw-Hill Publishing Company Ltd. New Delhi, 1976], can be obtained by simplifying the fine structure constant for the complex material.

[b] The effective atomic number, $Z_{eff} = \sqrt[2.94]{f_1 \times (z_1)^{2.94} + f_2 \times (z_2)^{2.94} + f_3 \times (z_3)^{2.94} + \cdots}$.

[c] Electron density (electrons/cm^3) of the material can be calculated using the approximate relation, $n_e = Z_{eff} \frac{N_A \rho}{M}$, where N_A is the Avogadro's number (6.023×10^{23}), ρ is the density, and M is the molecular weight of the complex.

[d] Plasmon energy (eV) of the complex system can be calculated using the relation $E_p = \left[\hbar \left(\frac{4\pi e^2}{m}\right)^{1/2}\right] (n_e)^{1/2} = 3.711 \times 10^{-11} \sqrt{n_e}$.

[e] Average binding energy of carbon 1s (PET) published in the paper [77].

As stated in the hypothesis, during Compton process the material target behaves as a virtual metamaterial, the NRI of PET ($\in$= 3.4) was estimated to be -0.52 (using expression (6)). Due to the NRI of the target material, x-rays of low frequency were scattered with high frequency (low wavelength). Wavelength shift in this process is found to be 0.0320Å experimentally for the PET, which matches well with the theoretically (using expression (10)) calculated value and is given in the Table 1. The intensity ratio (de-smeared data) of the modified (Compton) to unmodified, i.e., I_c/I_r $(=R_c)$ was found out to be 1.479. However, the Compton peak-to-background ratio obtained was about 68:1. It is interesting to note that a low-intensity peak of about 26.5% of the height of the Compton peak with the standard deviation, σ [70, 92] of 1.57% was visible on the high-energy side (with respect to coherent peak) of the spectra measured on PET. Intensity ratio of the above new incoherent peak I_a with usual unmodified peak I_r, i.e., I_a / I_r was found to be 0.394 (peak-to-background

ratio is 18:1). The position of this new peak corresponded to an energy transfer of about 123 eV(high energy side of the $CoK_{\alpha 1}$ line), whose Compton shift energy of about 138 eV (low energy side of the $CoK_{\alpha 1}$ line). However, the C1s binding energies of PET are 284.4 eV (benzene ring), 286 eV (-CH_2-O-) and 288.5 eV (-CO-O-) [93].

It is interesting to note that the Compton profile $J(q)$ from these 1s electrons was too weak to be observed, since the energy loss in the Compton process $\Delta\hbar\omega$ is less than the binding energy of the electron E_B. This ground state energy with 1s hydrogenic wave function at its initial-state can be written as $E_B = Z^2me^2/2\hbar^2$ [2]. The effective atomic number Z_{eff} , of the complex material (PET) can be calculated using the methods known as "self- consistent field (SCF)" or Hartree-Fock (HF) method, but in simplified situation $Z_{eff} = \sqrt[2.94]{f_1 \times (z_1)^{2.94} + f_2 \times (z_2)^{2.94} + f_3 \times (z_3)^{2.94} + \cdots}$, where f_1 is the fraction of the total number of electrons associated with each element and z_n is the atomic number of each element in the complex material [94]. Hence, the ground state velocity of the electron in terms of velocity of light was calculated to estimate the peak broadening. The energy spread of the new peak, i.e., width (38 eV) found out to be less than the Compton profile width (78 eV). Taking width of the profile into consideration, the energy of the incoherently scattered photon of Compton type (equation (24)) was found out to be 6.874 keV and energy of the new x-ray photon (equation (40)) is about 7.008 keV.

It was under these scattering conditions ($CoK_{\alpha 1}$ radiation and $2\theta = 109.5°$), the profile functions q and q' were calculated for both types of scattering process. The value of q and q' was found out to be +0.952 a.u. and +0.454 a.u., respectively. The negative sign of the expression (33) implies that for positive q value the energy shift is lower. Therefore, smaller the positive value of q, smaller will be the energy shift. Hence, the less positive value of q' (expression (43)) with respect to q (expression (33)) indicates that the energy exchange in the new process is lower as compared to the Compton process. The momentum transfer k_p in this process is found out to be 5.71 ± 0.02 $Å^{-1}$. The total scattering cross section σ_N, which is inversely proportional to the third power of the k_p (equation (76)), is found to be $(44.88 \pm 2.76) \times 10^{-24}$ cm^2/electron. This is very close to the theoretically calculated result ($(42.50 \pm 2.43) \times 10^{-24}$ cm^2/electron), and is given in the Table 1. Again, σ_N is directly proportional to $\sqrt{\in}$ as given in equation (76), which indicates that the materials of high value of dielectric constant produces high value of σ_N.

Most polymers possess very low value of static dielectric constant; this can be further enhanced in various ways. One of the important ways for enhancing the static dielectric constant (impurity free) of the polymer is by treating the polymer with proton beam [95–97].

5.1.2. Liquid glycerin

$CuK_{\alpha 1}$ (8.048 keV) x-ray scattered from 2 mm thick pure glycerin ($C_3H_8O_3$) shows the existence of this new peak. The sample was packed in a special-type liquid cell (25×30 mm^2) having 3 micron Mylar window at both sides. With an exposure of 10 h at 30 kV and 20 mA at scattering angle 108.5°, and effective area of 83 mm^2, the total spectrum was collected with a scanning speed of 0.00112 °/s. Intensity of the raw data was on the order of 10^4 scattered photons and the smeared intensity was about a few hundred counts from the liquid target, as shown in Figure 6. Though difficult, it is very interesting to analyze the gaseous and liquid samples [98, 99]. The Compton effect of other high-dielectric liquid-like water has been well studied [37, 100–104]. Because of the presence of carbon atom, high dielectric ($\in = 68$) nature, and availability in its pure form, glycerin was selected for the present study.

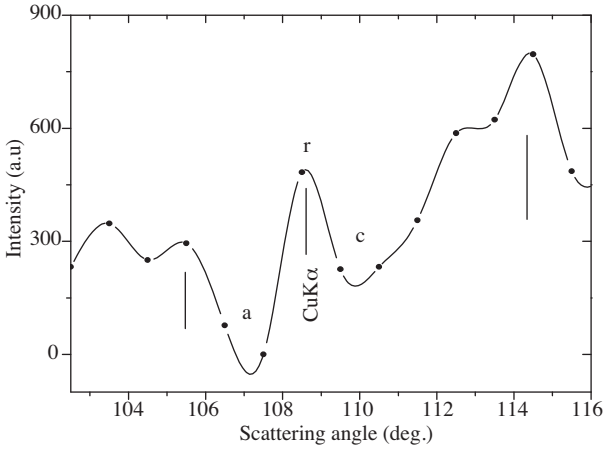

Figure 6. WDXR scattering spectra (accumulation of 10 h) of de-smeared intensity data obtained from glycerin at 108.5° using $CuK_{\alpha 1}$ line.

Table 2 shows the results of the glycerin-$CuK_{\alpha 1}$ scattered-profile. The wavelength shift of the Compton peak was calculated to be about 0.0285 Å. Since the dielectric constant is very high (about 68.2), the NRI was estimated to be -2.33. Because of very low NRI value, x-ray of low frequency scattered with high frequency (low wavelength). Experimental wavelength shift in this process is found to be 0.0296 Å. The intensity ratio of the modified (Compton) to unmodified peak, *i.e.*, I_c/I_r $(=R_c)$ was found out to be 1.629. A low-intensity peak similar to the peak found on the scattered profile of PET was observed with accuracy corresponding to 36.9 ± 2.05 % of the height of the Compton peak. The Compton peak-to-background ratio obtained was about 80:1. However, the ratio of this new peak-to-background is 35:1. Intensity ratio of the above new peak with usual unmodified peak I_a/I_r was found to be 0.663. The position of this new peak corresponded to an enhanced energy of about 140 eV with respect to the $CuK_{\alpha 1}$ line, whose Compton shift was about 163 eV. However, the electronic binding energies of glycerin are 286.1 eV (C 1s) and 532.2 (O 1s) [105]. Experimentally, the width of the Compton profile (116 eV) was found out to be more than the new incoherent profile (50 eV). The incoherently scattered photon energies $\hbar\omega_2$ and $\hbar\omega_3$ are found out to be 7.994 keV and 8.162 keV, respectively. The profile functions q and q' were calculated for both types of scattering process and were found out to be +1.219 a.u. and +0.519 a.u., respectively. This confirms that the energy exchange in the new process is lower as compared to the Compton process. The small momentum transfer k_p in this process is found out to be 6.60 ± 0.04 $Å^{-1}$. This gives a total scattering cross section σ_N of about (139.74 ± 1.81) $\times 10^{-24}$ cm^2/electron, which matches well with the theoretically calculated value ((129.93 ± 0.81) $\times 10^{-24}$ cm^2/electron). The high value of scattering cross section as compared to the PET sample is because of its high dielectric constant. This is one of the key parameters to observe this type of incoherent scattering phenomena, since the total scattering cross section is directly proportional to $\sqrt{\in}$ as given in equation (76).

5.2. EDXRF spectral analysis

Secondary x-ray of two different energetic lines PbL_{α} and MoK_{β} were used to obtain sufficiently extended scattering data. As discussed earlier, the actual interest of the study is on scattering of low-energy x-rays energy (<15 keV) in the non-relativistic region from the materials. X-rays of K, L and M lines of a particular element

show a decreasing order of energy and FWHM. From the table [46] related to wavelength of the spectral line of important target metals and their respective spectral line width, it is clear that the AgL x-ray lines are having the highest spectral resolution ($FWHM/\lambda$) and the PbL shows the next to the AgL lines. However, the PbL x-ray was selected to carryout the scattering experiment for many reasons. Firstly, the wide energy spacing between the two nearby PbL x-ray lines, i.e., the energy spacing between PbL_α-PbL_β or PbL_β-$PbL_{\gamma 1}$ is around 2.1 keV. Hence, the incident x-ray lines (PbL_α, PbL_β, $PbL_{\gamma 1}$), their respective Compton lines, SiK_α-escape peaks (from the Si(Li) detector) and the new incoherent line can be well separated. Nevertheless, the energy spacing between AgL_α-AgL_β or AgL_β-$AgL_{\gamma 1}$ is around 270 eV. Secondly, these x-ray lines (PbL x-ray lines) belongs to the non-relativistic photon (<15 keV) of maximum energy. Therefore, the maximum energy loss in the Compton collision process in a back scattering geometry is around 800 eV, which is expected to produce well-intense and well-separated peak for lighter elements (smaller Z).

Table 2. Analysis of $CuK_{\alpha 1}$ x-ray scattered profile from liquid glycerin applying WDXR spectrometry.

Parameter	Experimental value	Parameter	Experimental value
γ	0.016	$\in$	68.2
2θ /°	108.5	n (6)	±2.33
v/c	0.061	Z_{eff}	8.4
λ / Å	1.54056	n_e /10^{22} e/ cm^3	6.93
$\hbar\omega_1$/ keV	8.048	E_p /eV	9.77
$\hbar\omega_2$/ keV (24)	7.994	E_B^a /eV	13.6 (H 1s) 286.1 (C1s), 532.2 (O1s)
$\hbar\omega_3$/ keV (40)	8.162	I_a /I_r	0.663
q / a.u (33)	+1.219	I_c /I_r	1.629
q'/ a.u (43)	+0.519	I_a /R_c	198.59
$\Delta\lambda_c$/Å (25)	0.0285 ± 0.0003 (E) 0.0320 ± 0.0001 (T)	k_p /Å^{-1} (76)	6.60 ± 0.04 (E) 6.76 ± 0.04 (T)
$\Delta\lambda_N$/ Å	0.0296 ± 0.0003 (E) 0.0320 ± 0.0003 (T)	σ_N/10^{-24} (76) cm^2/electron	139.74 ± 1.81 (E) 129.93 ± 0.81 (T)

[a] Binding energy of 1s carbon and oxygen present in glycerin published in the paper (Krebs *et al.*, 2007).

5.2.1. Graphite

Pressed graphite powder pellet of 3 mm thick and 30 mm diameter was used to study the scattering profile of PbL x-rays. Data were collected at a 125° scattering angle and the running time of the total spectrum was about 20 h. The PbL x-ray [106, 107] spectrum scattered from graphite is shown in Figure 7(a). The PbL_α x-ray intensity of the Compton scattered photons was of the order of 1.5×10^4. However, graphite has been widely studied by various researchers [1, 2, 7, 9, 108–111] because of its small atomic number, low binding energy, simplicity, nontoxicity, low-price, and readily availability. As in earlier wavelength-dispersive

scattered-profiles (PET and glycerin), incoherent scattering peak of higher energy as compared to the incident PbL_α line of energy 10.5005 keV (channel number 806) was also observed.

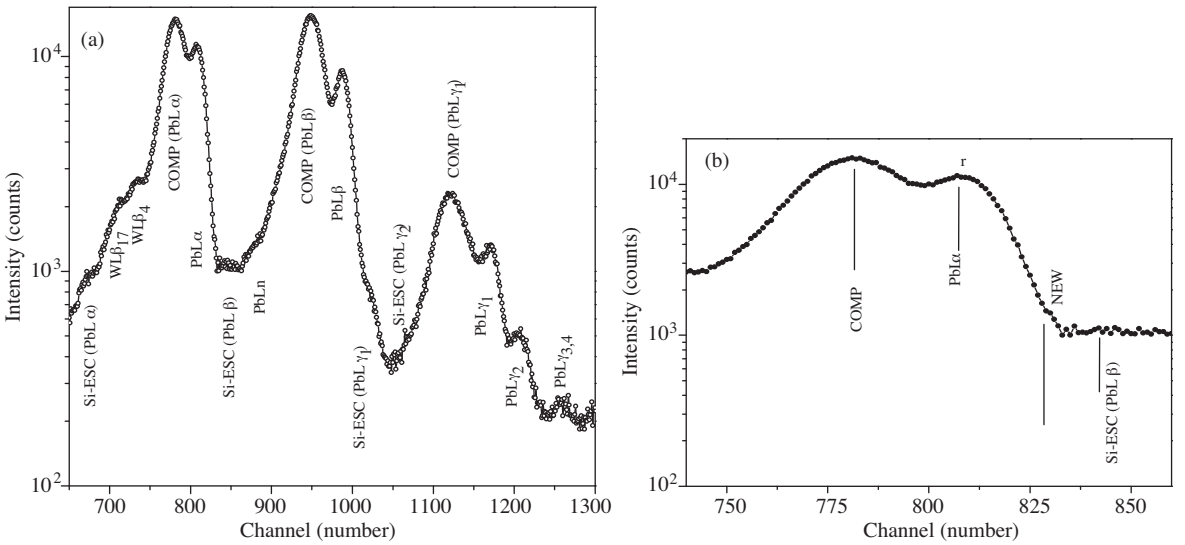

Figure 7. (a) Full EDXRF spectra (accumulation of 20 h) obtained from graphite pellet using PbL x-rays scattering at 125°, and (b) the enlarged part of the same spectra showing unmodified PbL_β line ($\boldsymbol{r}$), Compton (COMP) and the new-type incoherent scattering (NEW) line.

The energy shift of the Compton peak was calculated to be 325 eV with an average energy spread of about 13.03 eV per channel. The NRI of graphite ($\in$ = 12.15) was calculated and found out to be -0.977. Experimental energy shift in this process is found to be 300 eV, which is less than the energy absorbed in Compton process and is given in Table 3.

The intensity ratio of the modified (Compton) to unmodified peak, i.e., I_c/I_r $(=R_c)$ was found out to be 1.501. The Compton peak-to-background ratio obtained was about 403:1. A very low-intensity peak (at channel no. 829) of the new incoherent line followed by Si-ESC (PbL_β) was observed (incident PbL_β line of energy 12.618 keV occurs at channel no. 988), as shown in Figure 7(b). The peak-to-background ratio of the above line is about 39:1, with an accuracy corresponding to 9.5 $\pm$ 0.09 % of the height of the Compton peak. Again, the low- intensity PbL_n line of energy 11.349 keV [107] was observed at channel number 870, just after the Si-ESC (PbL_β) line. Intensity ratio I_a/I_r was found to be 0.057, which is quite less as compared to the CoK_α and CuK_α x-rays because of the greater photon emitting capacity of the high-power seald-off tube. This is because of the fact that PbL_α line is relatively more energetic then those x-rays. The peak is not an escape peak of the silicon (detector), since the energy displacement of the SiK_α escape peak from its incident x-ray peak is generally reported to be 1.740–1.755 keV [112, 113]. Again, the intensity ratio of escape peak to total peak is reported to be 4.4×10^{-3} [113]. The incoherently scattered photon energies $\hbar\omega_2$ and $\hbar\omega_3$ are found out to be 10.283 keV and 10.753 keV, respectively. Both the profile functions q and q' were calculated and were found out to be +0.858 a.u. and +0.692 a.u., respectively, which confirms that the energy exchange in the new process is lower as compared to the Compton process.

The small momentum transfer k_p in this process is found out to be 9.73 $\pm$ 0.03 $Å^{-1}$. This gives a total scattering cross section σ_N of about (320.44 $\pm$ 1.15) $\times10^{-24}$ cm^2/electron, which matches well with the

Table 3. Analysis of PbL_α x-ray scattered profile from the graphite powder applying EDXRF spectrometry. The factors used for the conversion of wavelength (Å) and energy (keV) is λ (Å) = 12.372/E (keV).

Parameter	Experimental value	Parameter	Experimental value
γ	0.021	$\in$	12.15
2θ /°	125	n (6)	±0.977
v/c	0.044	Z_{eff}	6
λ /Å	1.18075	n_e /10^{22} $e_/$ cm^3	67.2
$\hbar\omega_1$/ keV	10.5005	E_p / eV	30.42
$\hbar\omega_2$/ keV (24)	10.283	E_B^b/eV	284.2 (C1s),
$\hbar\omega_3$/ keV (40)	10.753	I_a /I_r	0.057
q / a.u (33)	+0.858	I_c /I_r	1.501
q'/ a.u (43)	+0.692	I_a /R_c	298
$\Delta\hbar\omega$/ eV (13)	325 ± 2.45 (E) 329 ± 0.88 (T)	k_p/Å^{-1} (76)	9.73 ± 0.03 (E) 9.76 ± 0.03 (T)
$\Delta\hbar\omega\|_N$ / eV [a]	300 ± 4.59 (E) 328 ± 9.23 (T)	σ_N/10^{-24} (76) cm^2/electron	320.44 ± 1.15(E) 315.74 ± 1.15(T)

[a] Theoretically the amount of energy transferred to x-ray photon by excited electron can be given in the energy dispersive relation $\Delta\hbar\omega|_N = \hbar\omega_3 - \hbar\omega_1 = \left(\frac{12.372}{\lambda - \Delta\lambda_N}\right) - \hbar\omega_1$, where $\Delta\lambda_N$ can be calculated using equation (9).
[b] The binding energy of carbon 1s [49].

theoretically calculated value ((315.74 ± 1.15) $\times 10^{-24}$ cm^2/electron). Since energy of the PbL_α line is high as compared to $CoK_{\alpha 1}$ line, one would expect low value of σ_N for PbL_α line. However, higher value σ_N for PbL_α line scattered from graphite is because of its high electron density (10^{23} electron/cm^3) and relatively high dielectric constant as compared to PET solid.

5.2.2. Single crystals (NaCl, MgF_2)

MoK radiation (secondary x-ray) based EDXRF system was used to analyze the single crystals and the pressed powder. The same graphite sample, which was studied using PbL x-rays, was also used. The single crystal slices of NaCl (100) and MgF_2 (110), about 3 mm thickness and 30 mm diameter, were used. The full spectrum of MoK radiation scattered at 90° from pressed-powder graphite pellet is shown in the Figure 8(a). In addition, MoK x-rays scattered at 90° from both the single crystals. Since there is no x-ray line after the MoK_β (20 keV) radiations, so this line was selected for analysis of the scattered-profile for the entire sample and is shown in Figure 8(b). The running time of the total spectrum of graphite was about 10 h, which produces intensity of MoK_α-Compton line is of the order of 10^5 scattered photons. However, the running time for the NaCl and MgF_2 single crystals were about 8 h each. A very low-intensity peak was observed at channel no. 618, which is about < 1 % of the height of the Compton peak. The lowest background of 610 counts was obtained at channel no. 236. For the $MoK_{\beta 1}$ x-rays, the Compton peak-to-background ratio is about 81:1. Intensity ratio with respect to unmodified ($MoK_{\beta 1}$) line, i.e., I_a/I_r was found to be very less, which is nearly 15 times less then the PbL_α line. This is because of the fact that $MoK_{\beta 1}$ (19.608 keV) line is relatively more energetic than the PbL_α (10.5005 keV) line. Experimental energy shift $\Delta\hbar\omega$ in the Compton scattering was found out to be

724 eV with energy spread of about 32.85 eV per channel and for the new process, the shift $\Delta\hbar\omega|_N$ is about 689 eV. Since energy of the incident-photon ($\mathrm{MoK}_{\beta 1}$) is greater than 15 keV, the relativistic effect comes into picture. The width of the Compton profile w_C is estimated to be less as compared to the profile w_N of new incoherent peak. Hence, for high-energy incident photon, the width of the profile becomes large with decreased intensity; therefore, the peak vanishes. This is another reason why this type of incoherent peak is not detected by the researchers working on Compton scattering using high-energy x-ray photons. Similarly, more energetic (as compared to the incident $\mathrm{MoK}_{\beta 1}$ line) and very low-intensity scattered peak was also observed from the NaCl (channel no. 618) and MgF_2 (channel no. 620) single crystals. However, detailed Compton scattering studies of NaCl [114, 115] and MgF_2 [116, 117] have been reported elsewhere.

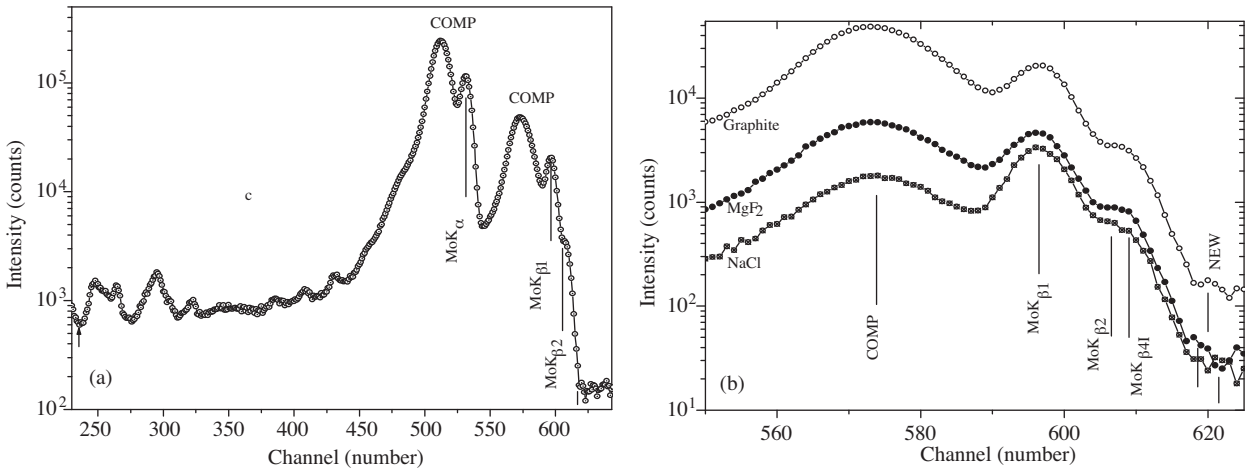

Figure 8. (a) Full energy spectrum (accumulation of 10 h) of MoK X-radiation scattered from powder graphite (pellet) at 90° using an EDXRF system, and (b) x-ray scattering spectra obtained from graphite (above), NaCl (100) and MgF_2 (110) at 90° using MoK_β X-radiation showing Compton modified (COMP), unmodified ($\boldsymbol{r}$) and new modified peak (NEW) are represented.

From the above studies on interaction of radiation with target materials, it was observed that this new x-ray effect can be observed using photons of energy of the order of 10 keV. A theoretical plot of energy shift $\Delta\hbar\omega|_N$ with scattering angles by 10 keV photons is shown in Figure 9(a). The maximum energy shift $\Delta\hbar\omega|_N$ at highest scattering angle 180° is about 300 eV. Again, the intensity ratio of modified (Compton) to unmodified peak, i.e., $I_c\,/\,I_r$ $(=R_c)$ is inversely proportional to the electronic binding energy of the material. The intensity ratio of new modified peak (at scattering angle around 90°–110°) with respect to R_c (selected to prevail over the effect of intensity ratio due to electronic binding energy of different materials), i.e., $I_a\,/\,R_c$ increases with increase in NRI value, as shown in Figure 9(b). This confirms that the material having high NRI value possesses more prominent peak. Again, the intensity ratio of new modified peak (in a carbon system) with respect to unmodified peak, i.e., $I_a\,/\,I_r$ decreases with increase in photon energy, as shown in Figure 9(c). A theoretical plot of differential scattering cross section $\left(\frac{d\sigma}{d\Omega}\right)_N$ for maximum scattering angle (180°) from a graphite system was plotted using x-ray photons of energy up to 100 keV, as shown in Figure 9(d). For 10 keV and 100 keV photon the theoretical cross section was calculated to be 2.187×10^{-23} cm^2/sr and 2.187×10^{-27} cm^2/sr respectively. On the other hand, comparison with Compton cross section, the new cross sections σ_N at 10 keV

and 100 keV are found out to be $10\sigma_C$ and $\sigma_C/100$ respectively. The experimental $\left(\frac{d\sigma}{d\Omega}\right)_N$ values of the PbL_α (10.5005 keV) line and $MoK_{\beta 1}$ (19.608 keV) line scattered by graphite and marked as dark-circle were also plotted. Both theoretically calculated and experimentally observed data match well with each other. A small deviation in the experimental data point of about 20 keV is because of the low scattering angle ($2\theta = 90°$).

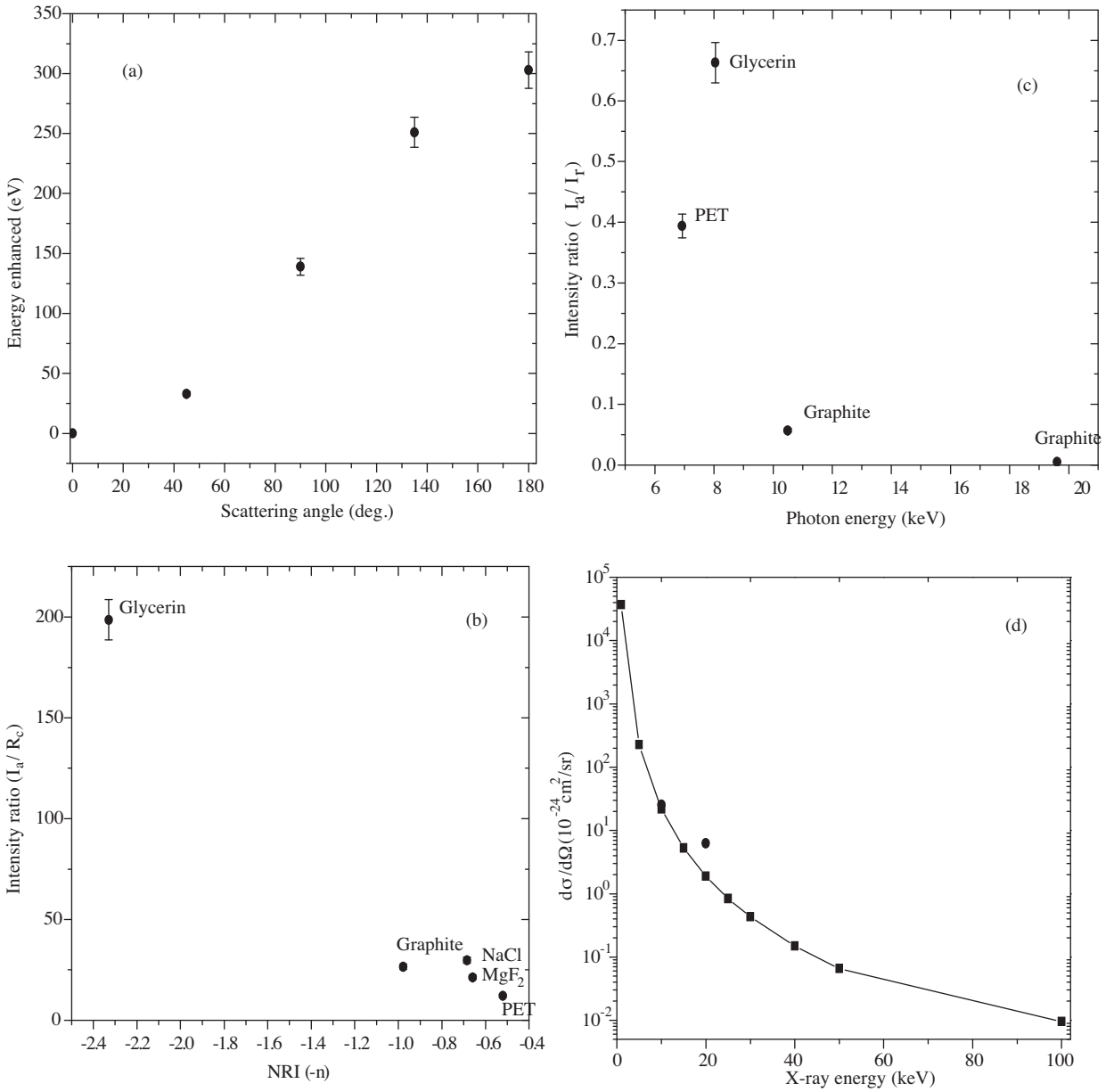

Figure 9. (a) Scattering angle (2θ) versus amount of energy enhanced by x-ray (10 keV) scattering at 180° from graphite in the new scattering process, (b) NRI ($-n$) versus I_a/R_c of materials of different dielectric constants, (c) incident photon energy versus I_a/I_r in high carbon materials, and (d) incident photon energy (1–100 keV) versus differential scattering cross section of the new scattering phenomena.

Usually, x-ray scattering from plasmon appears clearly under the condition that k is smaller than a critical wave vector k_c, i.e., $k < k_c$, As the case of the dielectric of our interest, $\varepsilon(\omega, k) < 0$ (where ω is real

and k is imaginary), the wave is damped with a characteristic length $1/|k_c|$ (plasmon cut-off vector). Higher value of this traditional plasmon cut-off wave vector k_c $(= 0.47 \times \sqrt{r_s}\ k_F)$ has been reported in Srivastava [118]. Indeed, x-ray scattering from plasmon with $k > k_c$ has been experimentally observed [58, 59, 119]. This large value of the damping constant is because of quadratic dispersion of RPA Lindhard type dielectric constant [120]. In addition, the plasmon dispersion curve bent over for larger values of k and showed little dependence of ω and k. This region of little dispersion occurred for k values well beyond k_c [119]. This is why the dynamic dielectric function $\varepsilon(\omega, k)$ replaced in terms of static dielectric constant $\in$ in equation (68). Hence, experimental observation of high value of k_p, i.e., $k_p > k_c$, in the final expression for the scattering cross section (76) is logical.

The relatively low-energetic x-rays used in this study limit the analysis of advance material systems like quantum dots [121], superconductors [122], disordered alloys [123–127], ferromagnetic amorphous alloys [128], and mixed crystals [129], as analyzed using the high-energy Compton scattering experiment. Also, the researchers of our Institute have been reported a number of good works on Compton profile and electron momentum density studies of many advance material systems for last three decades [114, 116, 129–133]. Hence, at low photon energies the "impulse-approximation" approach [134], which requires the energy transfer in the scattering process to be large, compared to the E_B involved, ceases to be valid for high-Z atoms. Again, the properties of electrons in solids can be better understood in the region of smaller energy and momentum transfer, since x-ray Compton spectra are very sensitive to band structure near the Fermi level. Hence, the new x-ray effect may give better understanding about the solid-state physics of the material and it is expected that this new effect will give a new dimension to understand the electronic structure of materials in general using the Compton effect.

6. Conclusion

In the present paper, theoretically predicted and experimentally observed new modified x-ray peak having the following major features has been reported: (i) the new modified peak is slightly less wide than the Compton peak because the modified peak width decreases with increase in frequency and strongly depends on scattering angle and amount of energy transfer; (ii) energy of the new modified peak is greater than that of Compton peak for the same incident x-rays; (iii) energy shift in this collision process is less than the shift by Compton process; and (iv) high value of total scattering cross section σ_N was obtained from materials of high dielectric constant and low binding energy on applying low-energy x-rays.

It has been reported that the Compton spectrometers have the best momentum resolution typically operated at about 10 keV, which means that the energy transferred to the Compton electron is of the order of 1 keV (i.e., the same order of magnitude as the binding energies of inner-shell electrons of light elements) [135]. It is expected that, with the use of relatively less harder x-rays, high-intensity x-ray source (synchrotron), x-ray detectors of excellent energy resolution [136, 137], position-sensitive detector [74, 108], imaging plate [74], suitable scattering angles (considering the plasmon scattering at $n_c < n_e$) [84] and materials (possessing low atomic number, high dielectric constant or metamaterials), it may be possible to get more prominent new modified peak with better signal-to-noise ratio. The instrument required for this purpose should be sensitive (Compton effect) to the polarization of x-ray considering all the geometrical factors.

Where polarization sensitivity of the device is a measure of asymmetry parameter A, and is a function

of asymmetry ratio R (ratio of cross sections) and N_R (ratio of coincidence counting rates) for high-energy Compton scattering study [138–141]. However, asymmetry parameter of low energy x-ray is given elsewhere [142, 143]. Therefore in the present WDXR instrument, the values of A are estimated as 0.037 ± 0.002 (CoK_α) and 0.046 ± 0.002 (CuK_α), using the theory suitable for the asymmetry of Thomson scattering spectrum (since Compton effect is less prominent in case of low energy x-ray) [143].

Similarly, for the EDXRF instruments, estimated values of A are 0.037 ± 0.003 (PbL_α) and 0.026 ± 0.002 (MoK_β) respectively. Advanced spectrometers such as dispersion-compensating [144] scanning x-ray spectrometer with high flux (in the order of 10^{11}–10^{12} photons/second) [145, 146], Cauchois-type x-ray spectrometer [147, 148], high resolution Compton spectrometer operated in the Rowland circular geometry [145] or better x-ray spectrometer for inelastic scattering [75, 149] are the right choice to carry out the studies. The inverse photoelectric effect (production of x-rays), the inverse Compton effect and the inverse Raman effect are the experimental processes for the production of new radiation, whereas anti-Stokes scattering is due to material mechanism, therefore the name of the new phenomenon may be proposed as anti-Compton scattering [43]. This new x-ray scattering can be applied for calculation of excited volume plasmon energy of materials [11], electron dynamics [150], or electron charge and spin density [151], valence-electron component of the atomic scattering factor [152], usual incoherent and coherent differential scattering cross-sections [153] within the same line as Compton effect, as well as for characterizing electroactive polymers, i.e., polymers of high-dielectric constant [154] and organic liquids, and for designing x-ray laser.

Acknowledgements

Author would like to express deepest thanks to Prof. N. Shiotani, Tokyo University of Fisheries, Tokyo; Prof. A. Bansil, North Eastern University, Boston, USA; Prof. Nobuhiko Sakai, Himeji Institute of Technology, Japan; and Prof. H. C. Padhi, Retired Professor of Institute of Physics, Bhubaneswar, India, for their discussion, criticism and suggestion on experimental work over the last few years. In addition, the author is indebted to Prof T. N. Tiwari, unique Research Centre, Rourkela, for reading and spending his valuable time to correct the contents of manuscript. My special thanks go to Prof. T. Patel, Prof. R. C. Behera, and Prof. S. Panigrahi of NIT, Rourkela, India for their help and encouragement.

Appendix A

The evaluation of the matrix element occurring in equation (55) requires multiplying $E' + \left(m_0c^2 + k_1\right)$ with numerator and denominator of the 1^{st} term of M, i.e., M_1. Using the wave equation,

$$E'\,u' \;= \left[(\alpha_i p') + \beta\, m_0 c^2\right]\; u' = H'\,u' \tag{A1}$$

where α_i, β are usual Dirac Matrices and p' is, of course, constant for the summation $\sum$:

$$|M_1| \;= \sum^{p'} \frac{(u^*\alpha\; u')\;\; (u'^*\alpha_0\; u_0)\;\; \left(m_0c^2 + k_1 + E'\right)}{E'^2 - \left(m_0c^2 + k_1\right)^2} \tag{A2}$$

$$|M_1| \;= \frac{\left[\left(m_0c^2 + k_1\right)\;\sum (u^*\alpha\; u')\;\; (u'^*\alpha_0\; u_0)\;\; + \sum (u^*\alpha\; H'\, u')\;\; (u'^*\alpha_0\; u_0)\right]}{E'^2 - \left(m_0c^2 + k_1\right)^2} \tag{A3}$$

Applying the general formula

$$\sum^{p'} \ (u_0^* Q_1 \ u') \ (u'^* Q_2 \ u) \ = (u_0^* Q_1 Q_2 \ u) \tag{A4}$$

and $E'^2 = p'^2 + \left(m_0 c^2\right)^2 = k_1^2 + \left(m_0 c^2\right)^2$, then

$$|M_1| \ = \frac{\left[\left(m_0 c^2 + k_1\right) \ (u^* \alpha \alpha_0 \ u_0 \ ) \ + (u^* \alpha \ H' \alpha_0 \ u_0 \ )\right]}{2 k_1 \ m_0 c^2}. \tag{A5}$$

Similarly, the 2^{nd} term of M, i.e., M_2 can be simplified using $E''^2 = p''^2 + \left(m_0 c^2\right)^2 = k_3^2 + \left(m_0 c^2\right)^2$ as

$$|M_2| \ = \frac{\left[E'' - \left(k_3 - m_0 c^2\right)\right] \ (u^* \alpha \ u'') \ (u''^* \alpha_0 \ u_0)}{\left(E''\right)^2 - \left(k_3 - m_0 c^2\right)^2}$$

$$|M_2| \ = \frac{\left[\left(m_0 c^2 + k_3\right) \ (u^* \alpha \ \alpha_0 \ u_0) + (u^* \alpha \ H'' \alpha_0 \ u_0)\right]}{2 k_3 \ m_0 c^2} \tag{A6}$$

Appendix B

Experimentally observed scattering intensity or the corrected yield Y_{corr} and can be defined as

$$Y_{corr} \ = n_p \ \sigma \ N_v \ l \ \frac{1}{\phi_s} \ \frac{1}{\phi_d} \ \frac{1}{\phi_{air}}, \tag{B1}$$

where n_p is the number of primary photon incident on the target, σ is the cross section, N_v is the number of atoms or molecules per cm^3, l is the sample thickness, ϕ_s is the self absorption factor in the target, ϕ_d is the detector efficiency and ϕ_{air} is the air absorption in the air column between detector window and target.

Applying quantum mechanical Klein-Nishin formula, the sensitivity of the Compton effect to the polarization of an incident x-ray can be estimated from the asymmetry parameter A, which is defined as

$$A = \frac{(1 - N_R \ R)}{(N_R - R)}, \tag{B2}$$

where $N_R = N_{\chi=90^\circ} / N_{\chi=0^\circ}$, is the ratio of the coincidence counting rates with the instrument set at angle χ and $R = d\sigma_{\chi=90^\circ} / d\sigma_{\chi=0^\circ}$ is the ratio of Compton scattering cross sections or asymmetry ratio and is given elsewhere [138].

However, for low energy x-ray the asymmetry parameter [143] of the Thomson scattering spectrum is given as

$$A = (v/c) \ \cos\phi, \tag{B3}$$

where ϕ is the angle between Compton recoil electron and scattered x-ray vector.

References

[1] A. H. Compton, *Phy. Rev.*, **21**, (1923), 409.

[2] L. V. Azaroff, R. Kaplow, N. Kato, R. J. Weiss, A. J. C. Wilson, and R. A. Young, X-ray Diffraction, ed. J. L. Farnsworth and J. W. Bradley, (McGraw-Hill, USA, 1974), p.1.

[3] L. Mendelsohn and V. H. Smith, Compton Scattering, ed. B. Williams (McGraw-Hill, Inc., Great Britain, 1977), p.102.

[4] C. V. Raman, *Nature* (London), **120**, (1927), 950.

[5] C. V. Raman, *Indian J. Phys.*, **3**, (1928), 357.

[6] C.V. Raman and C. M. Sogani, *Proc. R. Soc.* (London), A**119**, (1928), 526.

[7] S. Manninen, V. Honkimäki and P. Suortti, *J. Appl. Cryst.*, **25**, (1992), 268.

[8] R. J. Weiss and G. Mazzone, *J. Appl. Cryst.*, **14**, (1981), 401.

[9] K. Das Gupta, *Phy. Rev. Lett.*, **3**, (1959), 38.

[10] K. Das Gupta, *Phy. Rev.*, **128**, (1962), 2181.

[11] G. Priftis, *Phys. Rev.*, B**2**, (1970), 54.

[12] K. Das Gupta, *Phy. Rev. Lett.*, **13**, (1964), 338.

[13] E. E. Salpeter, *Phys. Rev.*, **120**, (1960), 1528.

[14] D. F. Dubois and V. Gilinsky, *Phys. Rev.*, **133**, (1964), A1308.

[15] D. F. Dubois and V. Gilinsky, *Phys. Rev.*, **133**, (1964), A1317.

[16] D. F. Dubois and V. Gilinsky, *Phys. Rev.*, **135**, (1964), A1519.

[17] P. M. Platzman, *Phys. Rev.*, **139**, (1965), A379.

[18] P. M. Platzman and N. Tzoar, *Phys. Rev.*, **139**, (1965), A410.

[19] P. Platzman and N. Tzoar, Compton Scattering, ed. B. Williams, (McGraw-Hill, Inc., Great Britain, 1977) p. 28.

[20] M. Jain and N. Tzoar, *Phys. Rev.*, A **18**, (1978), 538.

[21] G. R. Blumentha and R. J. Gould, *Rev. Mod. Phy.,* **42**, (1970), 237.

[22] G. B. Rybicki and A. P. Lightman, Radiative Process in Astrophysics, (Wiley, John & Sons, New York, 1985) p. 195.

[23] P. A. M. Gulchon and M. Vanderhaegben, *Prog. Part. Nucl. Phys.*, **41**, (1998), 125.

[24] N. Sakai, *J. Appl. Cryst.*, **29**, (1996), 81.

[25] W. Heitler, Quantum Theory of Radiation,ed. N. F. Mott, E. C. Bullard and D. H. Wilkinson, (The University Press. Oxford, 1960) p.110 & 211.

[26] P. M. Platzman, *Phys. Rev.,* B **40**, (1989), 5883.

[27] N. Seddon and T. Bearpark, *Science*, **302**, (2003), 1537.

[28] B. G. Williams, M. P. Parkison, C. J. Eckhardt and J. M. Thomas, *Chem. Phys. Lett.*, **78**, (1981), 434.

[29] B. G. Williams, T. G. Sparrow and R. F. Egerton, *Proc. R. Soc. Lond.*, A**393**, (1984), 409.

[30] P. Schattschneider and A. Exner, *Ultramicroscopy*, **59**, (1995), 241.

[31] B. G. Williams, M. K. Uppal and R. D. Brydson, *Proc. R. Soc. Lond.*, A**409**, (1986), 161.

[32] D. S. Su, P. Schattschneider and E. Zeitler, *Phys. Rev.*, B**49**, (1993), 8552.

[33] G. A. Sokol, The Nucleon Compton Effect at Low and Medium Energies, ed. D. V. Skobel'tsyn (Translated from Russian), Vol. 41 (Consultants Bureau . New York, 1969).

[34] P. A. M. Guichon, G. Q. Liu and A. W. Thomas, *Nucl. Phys.*, A**595**, (1995), 606.

[35] S. Capstick and B. D. Keister, *Phys. Rev.*, D**47**, (1993), 860.

[36] G. I. Watson, *J. Phys.: Condens. Matter.*, **8**, (1996), 5955.

[37] P. Zetterström, A. K. Soper and P. Schofield, *Physica*, B**234-236**, (1997), 337.

[38] H. D. Middendorf, U. N. Wanderlingh, R. L. Hayward and F. Albergamo, *Physica*, A **304**, (2002), 266.

[39] B. J. Gabrys, W. Jajac, J. Mayers and M. S. Kalhoro, *Appl. Phys.*, A**74**, (2002), S1645.

[40] C. A. Chatzidimitriou-Dreismann, M. Vos, C. Kleiner and T. Abdul-Redah, *Phys. Rev. Lett.*, **91,** (2003), 057403-1.

[41] Z.G. Pinsker, Dynamic Scattering of X-rays in Crystals, (Springer-Verlag, New York, 1981) p. 85.

[42] N. Shiotani, Personal communication (2001).

[43] B. Mallick, Proc. of the 87^{th} Ind. Sc. Cong. Young Scientist Award Abstract, Vol. III, (ISCA, Pune, India, 2000) p. 53.

[44] B. Mallick, Proc. of the 87^{th} Ind. Sc. Cong. Young Scientist Award Abstract, Vol. III, (ISCA, Delhi, India, 2001) p. 63.

[45] B. Mallick, Proc. SPIE Smart Structure and Materials, ed. Y. Bar-Cohen, Vol. 4329 (SPIE, California, 2001) p. 311.

[46] A. H. Compton and S. K. Allison, X-ray in Theory and Experiment, (D Van Nostrand Company, Inc; New York 1960).

[47] V. G. Veselago, *Soviet Phys. USPEKHI*, **10**, (1968), 509.

[48] A. C. Melissions, Experiments in Modern Physics, (Academic press, New York, 1973) p. 264.

[49] A.C. Thompson, D. Attwood, E. Gullikson, M. Howells, K.J. Kim, J. Kirz, J. Kortright, I. Lindau, P. Pianetta, A. Robinson, J. Scofield, J. Underwood, D. Vaughan, G. Williams and H. Winick, X-ray Data Booklet, ed. A.C. Thompson and D. Vaughan, (Lawrence Berkeley National Laboratory, University of California, Berkeley 2001) p. 5.21.

[50] C. Kittel, Introduction to Solid State Physics, (Wily Eastern Ltd., New Delhi, 1994) p. 289.

[51] J. Nilsen, W. R. Johnson, C. A. Jglesias and J. H. Scofield, UCRL-JRNL- 208675, (Lawrence Livermore National Laboratory, Berkeley 2004).

[52] G. E. M. Jauncey, *Phys. Rev.*, **25**, (1925), 314.

[53] G. E. M. Jauncey, *Phys. Rev.*, **25**, (1925), 723.

[54] J. W. M. DuMond, *Phys. Rev.*, **33**, (1929), 643.

[55] J. W. M. DuMond, *Rev. Mod. Phys.*, **5**, (1933), 1.

[56] E. H. Wichman, Quantum Mechanics, Berkeley Physics Course, Vol. 4, (The McGraw-Hill Companies Ltd., New Delhi, 2008) p.102.

[57] G. N. Fowler, Quantum theory, III Radiation and High Energy Physics, ed. D.R.Bates, (Academic Press, New York, 1962) p. 65.

[58] Y. Ohmura and N. Matsudaira, *J. Phys. Soc. of Japan*, **19**, (1964), 1355.

[59] N. G. Alexandeopoulos, *J. Phys. Soc. of Japan*, **31**, (1971), 1790.

[60] L.Von Hove, *Phys. Rev.*, **95**, (1954), 249.

[61] D. E. Parks and M. Rotenberg, *Phys. Rev.*, A**5**, (1972), 521.

[62] D. Pines, The Many-Body Problem, (Benjamin publications, New York, 1972).

[63] G. D. Mahan, Many-Particle Physics, (Kluwer Academic/ Plenum Publishers, New York, 2000).

[64] A. J. Glick, Lectures on the Many-Body Problem, ed. E. R. Caianiello, (Academic Press, New York, 1962).

[65] J. K. Laukkanen, PhD thesis, Helsinki University, Helsinki, Finland, 2000.

[66] E. Burkel, *J. Phys.: Condens. Matter*, **13**, (2001), 7477.

[67] P. M. Bergstrom and R. H. Pratt, *Radiat. Phys. Chem.*, **50**, (1997), 3.

[68] Y. H. Woo, *Phys. Rev.*, **25**, (1925), 444.

[69] T. Paakkari and P. Suortti, *Phys. Rev.*, B**9**, (1974), 1756.

[70] E. P. Bertin, Principle and Practice of X-ray Spectrometric Analysis, (Plenum press, New York, 1975).

[71] R. Tertian and F. Claisse, Principle of Quantative X-ray Fluorescence Analysis, (Heyden & Son Ltd; London, 1982) p. 336.

[72] Z. W. Chen, W. M. Gibson and H. Huang, *X-ray Optics & Instrum.* doi: 10.1155/2008/318171, (2008).

[73] W. R. McIntire, *Phys. Rev.*, B**14**, (1976), 4386.

[74] N. Shiotani, N. Sakai, F. Itoh, M. Sakurai, H. Kawata, Y. Amemiya and M. Ando, *Nucl. Instrum. Methods.*, A**275**, (1989), 447.

[75] P. Pattison, P. Suorti and W. Weyrich, *J. Appl. Cryst.*, **19**, (1986), 353.

[76] E. Straube, D. Hohlwein and Th. Zeiske, *J. Appl. Cryst.*, **31**, (1998), 169.

[77] B. D. Cullity, Elements of X-ray Diffraction, (Addition-Weseley Publishing Company, Inc. London, 1978).

[78] *Pro-Fit* software, Philips Analytical X-ray, Netherlands (1999).

[79] P. Pattion and J. R. Schneider, *Nucl. Instrum. Methods.*, **158**, (1979), 145.

[80] G. F. Knoll, Radiation Detection and Measurements, (John Wiley & Sons, New York, 1989).

[81] *AXIL,* X-ray analysis software, International Atomic Energy Agency, Austria (1993).

[82] R. D. Evans, The Atomic Nucleus, (McGraw-Hill Book Company, London, 1955).

[83] P. Holm, *Phys. Rev.*, A**37,** (1988), 3706.

[84] T. Suzuki and A. Tanokura, *J. Phys. Soc. of Japan*, **29**, (1970), 972.

[85] D. M. Miliotis, *Phys. Rev.*, B**3**, (1971), 701.

[86] S. L. McCall and P. M. Platzman, *Phys. Rev.*, B**22**, (1980), 1660.

[87] G. G. Cohen, N. G. Alexandropoulos and M. Kuriyama, *Phys. Rev.*, B**8**, (1973), 5427.

[88] W. Weyrich, P. Pattison and B. G. Williams, *Chem. Phys.*, **41**, (1979), 271.

[89] D. L. Anastassopoulos, G. D. Priftis, C. Toprakcioglu and A. A. Vradis, *Phys. Rev. Lett.*, **81**, (1998), 830.

[90] E. P. Mazarakiotis, D. L. Anastassopoulos, A. A. Vradis, G. D. Priftis, Ch. Bellin and G. Loupias, *Physica*, B**318**, (2002), 382.

[91] M. Abdelrahman and N. Kamel, *Jpn. J. Appl. Phys.*, **37**, (1998), 4563.

[92] R. Jenkins and J. L. de Vries, Worked Examples in X-ray Analysis, (The Macmillan Press Ltd; London, 1978).

[93] K. Ueno, Y. Matsumoto, N. Nishimiya, M. Noshiro and M. Satou, *Nucl. Instrum. Methods*, B**59/60**, (1991), 1263.

[94] R. C. Murty, *Nature*, **207**, (1965), 398.

[95] N. Saha, N. L. Singh, C. F. Desai and K. P. Singh, *Radiat. Meas.*, **36**, (2003), 699.

[96] N. L. Singh, N. Shah, K. P. Singh and C. F. Desai, *Radiat. Meas.*, **40**, (2005), 741.

[97] B. Mallick, T. N. Tiwari, S. Panigrahi and R. C. Behera, *Meas. Sci. Technol.*, **17**, (2006), 3289.

[98] P. Eisenberger, *Phys. Rev.*, A**2**, (1970), 1678.

[99] P. Eisenberger, *Phys. Rev.*, A**5**, (1972), 628.

[100] U. Bonse, W. Schröder and W. Schülke, *J. Appl. Cryst.*, **12**, (1979), 432.

[101] K. Nygård, M. Hakala, S. Manninen, A. Andrejczuk, M. Itou, Y. Sakurai, L. G. M. Pettersson and K. Hämäläinen, *Phys. Rev.*, **74**, (2006), 031503-1.

[102] K. Nygård, PhD Thesis, University of Helsinki, Helsinki, Finland 2007.

[103] T. Abdul-Redah, M. Krzystyniak and C. A. Chatzidimitriou-Dreismann, *Phys. Rev.*, B**72**, (2005), 052202-1.

[104] A. Shukla, B. Barbiellini, T. Buslaps and P. Suortti, *Zeitschrift fur Physikalische Chemie*, **215**, (2001), 1315.

[105] 5T. Krebs, G. Andersson and H. Morgner, *Chem. Phys.*, **340**, (2007), 181.

[106] H. Yamaoka, M. Oura, K. Takahiro, N. Takeshima, K. Kawatsura, M. Mizumaki, U. Kleiman, N. M. Kabachnik and T. Mukoyama, *Phys. Rev.*, A**65**, (2002), 062713-1.

[107] California Institute of Technology, X-ray.dat; http://www.pma.caltech.edu/∼dons/ph3-7/xray.dat (1997).

[108] P. Pattison, H-J. Bleif and J. R. Schneider, *J. Phys. E. Sci. Instrum.* (Great Britain), **14**, (1981), 95.

[109] G. D. Priftis and J. Boviatsis, *Phys. Lett.*, A**85**, (1981), 115.

[110] S. Vasudevan, T. Rayment, B. G. Williams and R. Holt, *Proc. R. Soc. Lond.*, A**391**, (1984), 109.

[111] F. F. Kurp, Th. Tschentscher, H. Schulte-Schrepping, J. R. Schneider and F. Bell, *Europhys. Lett.*, **35**, (1996), 61.

[112] G. Kalinka, *Nucl. Instrum. Methods,* B**88**, (1994), 470.

[113] T. Papp and J. L. Campbell, *X-ray Spectrom.*, **30**, (2001), 77.

[114] G. Das and H. C. Padhi, *Philos. Mag.*, B**54**, (1986), 415.

[115] R. Vijayakumar, Shivaramu, L. Rajasekaran, N. Ramamurthy, and M. J. Ford, *Nucl. Instrum. Methods*, B**234**, (2005), 185.

[116] G. Das and H. C. Padhi, *Phys. Lett.*, A**128**, (1988), 383.

[117] H. Lan, J. Yang and K. Wang, *Phys. Lett.*, A**144**, (1990), 419.

[118] K. S. Srivastava, *Solid State Commun.*, **30**, (1979), 19.

[119] K. L. Kliewer and H. Raether, *Phys. Rev. Lett.*, **30**, (1973), 971.

[120] H. J. Höhberger, A. Otto and E. Petri, *Solid State Commun.*, **16**, (1975), 175.

[121] R., Saniz, B. Barbiellini and A. Denison, *Phys. Rev.*, B**65**, (2002), 245310-1.

[122] W. Schulke, *IUCr Newsletter,* **1**, (1993), 6.

[123] A. Bansil, R. S. Rao, P. E. Mijnarends and L. Schwartz, *Phys. Rev.,* B**23**, (1981), 3608.

[124] A. Bansil and S. Kaprzyk, *Phys. Rev.*, B**57**, (1991), 314.

[125] A. Bansil, S. Kaprzyk, A. Andrejczuk, L. Dobrzyski, J. Kwiatkowska, F. Maniawski and E. ukowski, *Phys. Rev.*, B**57**, (1998), 314.

[126] D. Pal and H. C. Padhi, *Phys. Status Solidi.,* B**175**, (2006), 507.

[127] B. K. Shrma, V. Purvia, B. L. Ahuja, M. Sharma, P. Chaddah, S. B. Roy, Y. Kakutani, A. Koizumi, T. Nagao, A. Omura, T. Kawai and N. Sakai, *Phys. Rev.*, B**72**, (2005), 132405-1.

[128] J. W. Taylor, J. A. Duffy, A. M. Bebb, M. J. Copper, S. B. Dugdale, J. E. McCarty, D. N. Timms, D. Greig and Y. B. Xu, *Phys. Rev.*, B**63**, (2001), 220404-1.

[129] D. P. Mahapatra and H. C. Padhi, *Solid State Commun.*, **42**, (1982), 525.

[130] D. P. Mahapatra and H. C. Padhi, *J. Phys. Soc. Jpn.*, **42**, (1982), 525.

[131] B. K. Panda, *Phys. Rev.*, B**49**, (1994), 2521.

[132] B. K. Panda, D. Pal, D. P. Mahapatra, and H. C. Padhi, Positron Annihilation and Compton Scattering, ed. B. K. Sharma, P. C. Jain and R. M. Singru, (Omega Scientific Publishers, New Delhi, 1990) p. 297.

[133] D. Pal, PhD Thesis, Utkal University, Bhubaneswar, India, 1991.

[134] R. Currat, P. D. DeCicco and R. J. Weiss, *Phys. Rev.*, B**4**, (1971), 4256.

[135] S. Huotari, K. Hämäläinen, S. Manninen, S. Kaprzyk, A. Bansil, T. Buslaps, V. Honkimäki and P. Suortti, *Phys. Rev.*, B**62**, (2000), 7956.

[136] Princeton Gamma-Tech *(PGT)* Instruments Inc; X-ray Detectors, http://www.pgt.com/prods.html (2000).

[137] S. Barkan, V. D. Saveliev, P. Pianetta, S. Brennan, C. R. Tull, L. Feng, M. Takahashi, D. Burnett and H. Ishii, *(VORTEX),* Proc. European Conference on X-ray Spectrometry, http://www.siintusa.com/pdf/EXRS2008.pdf (2008).

[138] H. Schopper, *Nucl. Instrum.*, **3**, (1958), 158.

[139] L. W. Fagg and S. S. Hanna, *Rev. Mod. Phys.*, **31** (1959), 711.

[140] P. Taras and J. Matas, *Nucl. Instrum. Methods.*, **82** (1970), 173.

[141] G. E. Owen and Y. K. Lee, *Nucl. Instrum. Methods.*, **61** (1968), 317.

[142] C. Visñovesky, S. Limandri, M. E. Canafoglia, R. Bonetto and J. Trincavelli, *Spectrochem. Acta.*, B**62**, (2007), 492.

[143] Th. Wrubel, S. Glenzer, S. Büscher and H. –J. Kunze, *J. Atmos. Terre. Phys.*, **58**, (1996), 1077.

[144] P. Suortti, T. Buslaps, M. DiMichiel, V. Honkimäki, M. Kretzschmer, U. Lienert, J. E. McCarthy, J. M. Merino and A. Shukla, *Nucl. Instrum. Methods.*, A**467-468**, (2001), 1541.

[145] K. Hämäläinen, S. Manninen, C. –C. Kao, W. Caliebe, J. B. Hastings, A. Bansil, S. Kaprzyk and P. M. Platzman, *Phys. Rev.*, B**54**, (2000), 5453

[146] P. Suortti, T. Buslaps, P. Fajardo, V. Honkimäki, M. Kretzschmer, U. Lienert, J. E. McCarthy, M. Renier, A. Shukla, T. Tschentscher and T. Meinander, *J. Synchrotron Rad.*, **6**, (1999), 69.

[147] M. Itou, N. Hiraoka, T. Ohata, M. Mizumaki, A. Deb, Y. Sakurai and N. Sakai, *Nucl. Instrum. Methods.,* A**467-468**, (2001), 1109.

[148] Y. Sakurai and M. Itou, *J. Phys. Chem. Solids*, **65**, (2004), 2061.

[149] P. Suortti, P. Pattison and W. Weyrich, *J. Appl. Cryst.*, **19**, (1986), 336, 343.

[150] W. Schülke, Electron dynamics by inelastic X-ray scattering, (Oxford University press, Oxford, UK, 2007).

[151] M. Cooper, P. E. Mijnarends, N. Shiotani, N. Sakai and A. Bansil, X-ray Compton scattering, (Oxford university press, Oxford, UK, 2007).

[152] V. A. Bushuev, A. Yu. Kazimirov and M. V. Koval'chuk, *JETP Lett.*, **47**, (1988), 187.

[153] Y. Kurucu, S. Erzeneğlu, R. Durak and Y. Şahin, *Turk. J. Phys.*, **22**, (1998), 783.

[154] H. Cheng and Q. Zhang, Proc. Smart Structures and Materials 2004: Electroactive Polymer Actuators and Devices (EAPAD), ed. Y. Bar-Cohen, Vol. 5385 (SPIE, US, 2004) p. 87.